Papers presented at the

Second Annual

Summer Intern Conference

August 14, 1986
Houston, Texas

1986 Summer Intern Program for Undergraduates
Lunar and Planetary Institute

Papers presented at the

Second Annual
Summer Intern Conference

August 14, 1986
Houston, Texas

1986 Summer Intern Program for Undergraduates
Lunar and Planetary Institute

Co-sponsors: Lunar and Planetary Institute
NASA Johnson Space Center

Compiled by the
Lunar and Planetary Institute
3303 NASA Road One
Houston, Texas 77058

LPI Contribution 602

LPI Summer Undergraduate Intern Program

During the month of January each year the Lunar and Planetary Institute offers students world-wide an opportunity to work closely with scientists active in lunar and planetary research. Approximately 200 applications are received each year from qualified applicants who are college undergraduates. Out of these applicants, 12 to 14 students are chosen to take part in the Summer Undergraduate Intern Program. Scientists from the Lunar and Planetary Institute and the NASA Johnson Space Center direct the interns in a variety of research projects. Interns have the opportunity to present a profile of their research to their colleagues and advisors, and to interact with scientists from the Lunar and Planetary Institute, NASA Johnson Space Center and with visiting researchers from the lunar and planetary science community. Summer, 1986, is the tenth year of the Intern Program.

For additional information on this program contact the Projects Office, Lunar and Planetary Institute, 3303 NASA Road 1, Houston, TX 77058.

PROGRAM OF PAPERS PRESENTED AT THE SECOND ANNUAL

SUMMER INTERN CONFERENCE

Lunar and Planetary Institute
August 14, 1986
Houston, Texas

MORNING SESION
9:00 - 11:00 a.m.

Chairman: Bruce Bills

AFTERNOON SESSION
1:00 - 3:10 p.m.

Chairman: James Zimbelman

DIFFERENTIAL VOLATILIZATION OF LUNAR IMPACT GLASS USING RAYLEIGH FRACTIONATION MODELING Louis J. Boschelli, Department of Chemical Engineering, University of Illinois, Champaign; David S. McKay, Johnson Space Center, NASA

One effect that meteorite impacts have on the lunar surface is the heating of target rock above liquidus temperatures, causing partial vaporization. During the high temperature period associated with partial vaporization, different elements may volatilize at different rates, creating fractionated ejecta (glass spheres) (1,2,3,4).

Modeling of the impact vaporization process can be achieved with Rayleigh fractionation (3,5) which requires a well-mixed melt and vapor-liquid equilibrium. The Rayleigh equation for a multicomponent system is:

$$(m_i/m_{io})=(m_j/m_{jo})^{a_{ij}}$$

where i and j are liquidus components (eg., SiO_2, FeO), m_o is the component's initial mass, m is the component's mass after a period of vaporization, and a_{ij} is an empirical term representing the volatility of the ith component relative to the jth.

Lunar simulant glasses of known initial composition were heated on indented molybdenum strips in a vacuum bell jar ($P\sim10^{-5}$ torr) at temperatures of 1150°C, 1300°C and 1500°C. Runs of different duration were performed at each temperature, producing residues with varying amounts of mass loss.

Mixing of the melt during heating, necessary for Rayleigh fractionation, was confirmed by making multiple quantitative analyses of each melt residue. Residues were mounted in epoxy, polished, and analyzed on a JEOL-35CF scanning electron microscope equipped with a PGT System IV energy dispersive x-ray analyzer (EDXA). Data was then reduced with the DUSTPC program (6) (modified by D. Anderson and Tom Lin, NASA/JSC, pers. comm.). Results revealed the product glasses to be homogeneous.

The experiments at 1500° produced a consistent relative volatility sequence. The sequence observed was as follows: FeO > MnO > P_2O_5 > SiO_2 > MgO > Al_2O_3 > TiO_2 > CaO (CaO thus being the most refractory). Initial and final composition and weight data were used to calculate a_{ij} values for each component relative to an arbitrarily chosen reference component:

a_{FeOMnO}	$a_{FeOP_2O_5}$	a_{FeOSiO_2}	a_{FeOMgO}	$a_{FeOAl_2O_3}$	a_{FeOTiO_2}	a_{FeOCaO}
1.43	2.40	2.67	5.13	6.67	7.80	8.05

Figure 1

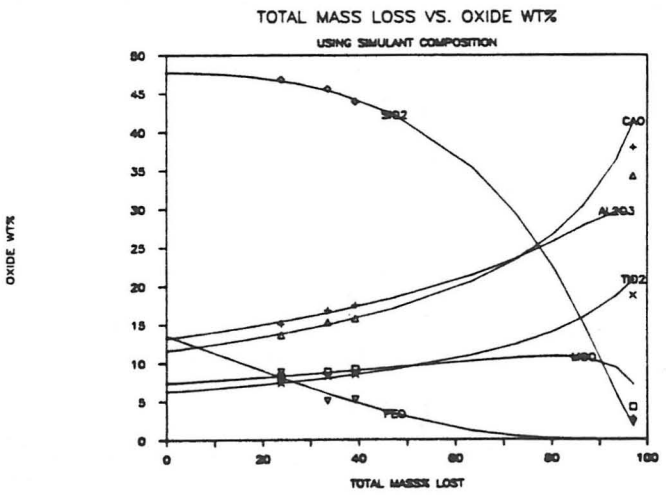

From the experimental a_{ij} values, a graph of oxide weight percent vs. total mass loss of the simulant glass was prepared with the assumption of constant relative volatility during the mass loss process. The fit of lunar simulant compositions to the theoretical curve demonstrates that Rayleigh fractionation occurred during the 1500° runs and that constant relative volatility is a valid assumption (fig. 1).

Runs at 1150° and 1300° did not produce data consistent with the fractionation model. As demonstrated by numerous researchers (7,8,9) the vapor phase of a lunar sample heated to less than 1400°C consists mainly of Fe and alkalis. Glass residues from 1150° and 1300° runs did show marked depletions in FeO while other substituents (SiO_2, CaO, MgO, etc.) remained unvolatilized to any measurable extent.

Oxide weight percent vs. total mass loss graphs were constructed for various Apollo 15 soil and rock starting compositions using the relative volatility data obtained at 1500°C. Compositions of lunar glass spheres from 15086,39 were obtained using EDXA analysis on polished thin sections. These sphere compositions were then individually fitted to the constructed Apollo 15 graphs with a least-squares analysis. Accurate fits provide estimates of the amount of mass lost from individual spheres during impact and the subsequent cooling period.

Many lunar spheres were found to fit the curves, suggesting that selective volatilization from well-mixed melts occurs frequently during the lunar impact process. Soil 15210, obtained from a work station near the 15086,39 sampling site, displayed the most fits (figs. 2,3). An anorthositic rock composition (15455) provided many fits (figs. 4,5), consistent with the observation that 80% of the lunar surface is of highlands composition (primarily anorthositic). Few sphere compositions matched the curve of the local regolith breccia (15086), which indicates that most impact glasses undergo significant transport during the impact event.

Comparison of cosmic dust compositions obtained via EDXA (e.g., W7029H10, W7029G11, W7029D14, W7029H9) (10) to the lunar fractionation graphs provided a number of fairly good fits, indicating that some cosmic dust entering the earth's stratosphere may have been ejected from the lunar surface via micrometeoritic impacts. Initial compositions in this case are more difficult to estimate, so fittings are neccessarily more qualitative in nature. Further research into the nature of these particles is needed for substantiation.

Figure 2

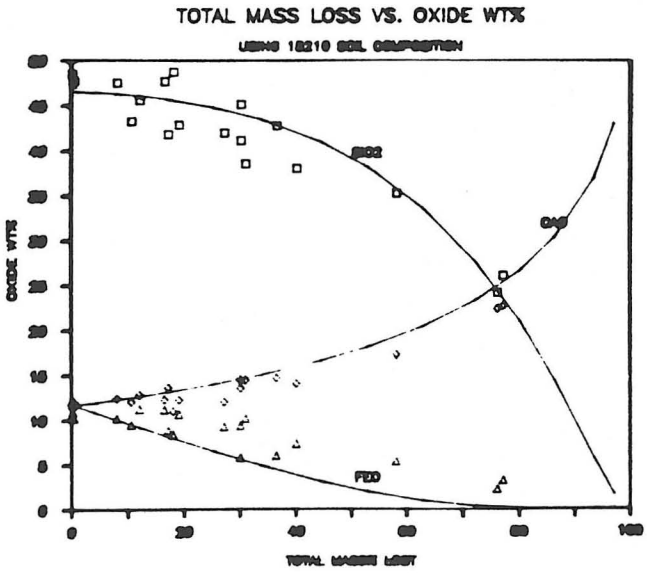

Figure 3

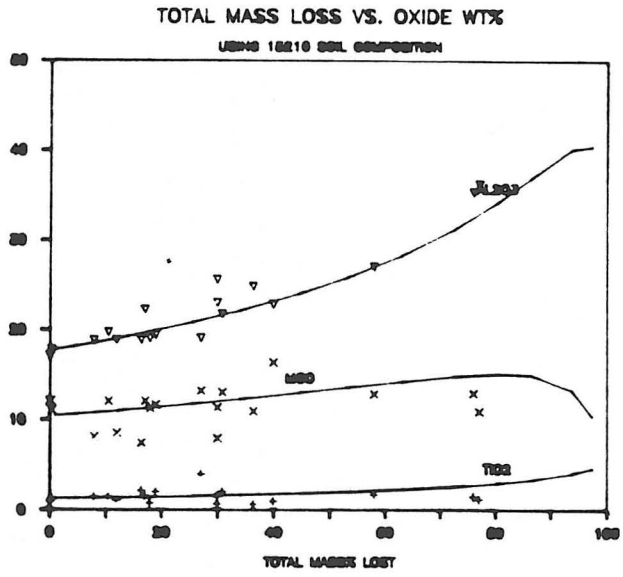

Figure 4

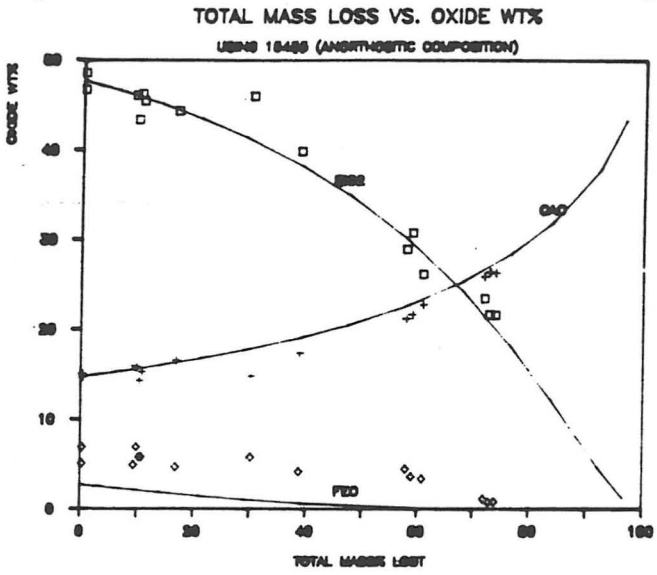

Figure 5

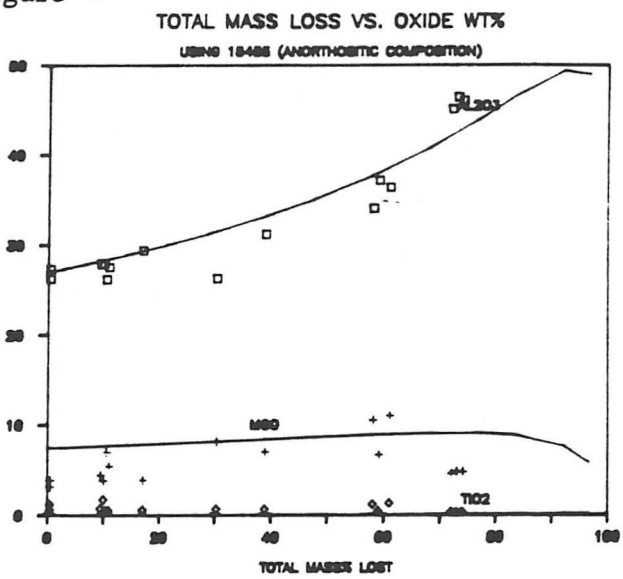

1. Horz, F., et. al. (1983) J. Geophys. Res., V. 88, Suppl., B353-B363.
2. Delano, J. W., ET. AL. (1981) Proc. L. P. S. C. V. 12th, 339-370.
3. Housley, R. M. (1979) Proc. L. P. S. C. 10th, 1673-1683.
4. Kempa, M. J., and Papike, J. J. (1980) Proc. L. P. S. C. 11th, 1635-1661.
5. Clayton, R. N., et. al. (1974) Proc. L. S. C. 5th, 1801-1809.
6. Armstrong, J. T., and Buseck, P. R. (1975) Anal. Chem. 47, 2178.
7. Gooding, J. L., and Muenow, D. L. (1976) Geo. Cosmo. Acta V. 40, 675-686.
8. Gooding, J. L., and Muenow, D. L. (1977) Meteoritics, V.12, #4, 401-406.
9. De Maria, G., et. al. (1971) Proc. L. S. C. 2nd, 1367-1380.
10. Clanton, U. S., et. al., (1983, 1984) NASA/JSC Cosmic Dust Catalogs.
11. Hashimoto, A. (1983) Geochemical J. V. 17, 111-145.

SYNTHESIS OF ILMENITE-HEMATITE SOLID SOLUTIONS AND THE KINETICS OF THEIR REDUCTION. R.A. Briggs, Department Chemical Engineering, Worcester Polytechnic Institute, Worcester MA 01545; R.J. Williams, Advanced Research Projects Office, Mail Code SN 12, NASA-JSC, Houston, TX 77058.

Iron-titanium oxides and their solid solutions, essentially ilmenite-hematite ($FeTiO_3$-Fe_2O_3) and ulvospinel-magnetite (Fe_2TiO_4-Fe_3O_4) provide a useful means of predicting the formation conditions of the rocks in which they occur. In particular, both the temperature and oxygen fugacity (fO_2) can be ascertained in favorable cases. This geothermometer/oxybarometer was introduced by Buddington and Lindsley [1] and later modified by Lindsley and Rumble [2]. Also important in the interpretation of these assemblages is an understanding of the kinetics and mechanisms of oxidation and reduction between the two solid solutions and their end members. The purpose of this study was two-fold - the synthesis of ilmenite-hematite solid solutions and a preliminary examination of their reduction kinetics.

Ilmenite-hematite solid solutions and pure ilmenite were synthesized under controlled temperature and fO_2 using CO-CO_2 gas mixtures. Two solid solutions $ilm_{70}hem_{30}$ and $ilm_{60}hem_{40}$, were synthesized for study. These compositions were chosen to bracket the Fe/Ti ratio of ulvospinel and thus to have different reaction sequences on reduction. Oxygen fugacity was monitored by a solid ceramic (Y_2O_3-ZrO_2) oxygen electrolyte cell with a precision of +0.1 log units [3]. Stoichiometric amounts of hematite and rutile (TiO_2) were ground together under acetone and pressed into pellets weighing approximately 100-125 mg. The pellets were placed into a Pt-wire basket and suspended in the furnace at the desired temperature and fO_2. After 24-48 hrs the pellets were extracted, reground, pelletized again, and placed back into the furnace. After a similar period of time x-ray powder diffraction analysis was performed to determine the solid products remaining. Ilmenite was synthesized at 1150°C; solid solutions were synthesized at 1050°C. Since the equilibrium fO_2 over the latter was not known, extrapolation from existing data [4] served as an initial estimate during their synthesis. If x-ray analysis showed the fO_2 to be too low (by the presence of ulvospinel - magnetite) or too high (by the presence of pseudobrookite), corresponding adjustments were made. By this process of synthesis, x-ray analysis, and fO_2 adjustment, the exact synthesis conditions of the samples were obtained. One pellet from each final sample was mounted and polished and examined for its iron and titanium distribution using backscattered electrons under a Cameca Camebex electron microscope. Finally, to determine the quantity of hematite in the ilmenite-hematite solid solutions, measurements of

the hkl = 024 and 116 plane peaks were taken using x-ray diffraction with fluorite (CaF_2) as an internal standard. After their synthesis and quantification, a preliminary examination of reduction kinetics was performed.

Kinetics of reduction of the ilmenite-hematite solid solutions were determined from weight loss of pelletized samples over time. Samples weighing approximately 100-125 mg were suspended in a Pt-wire basket in a $CO-CO_2$ gas flow furnace similar to that used during synthesis [3]. A Cahn electrobalance monitored the weight of the pellet over time. Experiments were carried out at 1080°C and an oxygen fugacity of -15.3 log units, 0.5 log units below the ilmenite to iron and rutile breakdown curve. From the fixed Fe/Ti ratios of the samples, the theoretical breakdown path could be constructed on phase diagrams. Comparisons to experimental results were made to determine the reduction sequence of these iron titanium oxides.

REFERENCES:

1. A.F. Buddington, D.H. Lindsley; Iron-titanium oxide minerals and synthetic equivalents. J. Petrol. 5 (1964) 310

2. D.H. Lindsley, D. Rumble III; Magnetite-ilmenite geothermometer oxybarometer: an evaluation of old and new data. EOS 58, 6 (1977) 519

3. R.J. Williams, O. Mullins; JSC system using solid ceramic oxygen electrolyte cells to measure oxygen fugacities in gas-mixing systems. NASA Tech. Mem 5824 (Johnson Space Center, Houston TX, 1981).

4. D.H. Lindsley; Equilibrium relations of coexisting pairs of Fe-Ti oxides. Carnegie Inst. Wash. Yearb. 62 (1963) 60.

VIKING HIGH-RESOLUTION THERMAL INERTIA INVESTIGATION OF THE THARSIS AND PHOENICIS LACUS QUADRANGLES, MARS. Ken Edgett, Earlham College Geology Department, Richmond, Indiana 47374. Advisor: J. R. Zimbelman, Lunar and Planetary Institute, Houston, Texas 77058.

Thermal inertia (units x 10^{-3} cal cm^{-2} $s^{-1/2}$ K^{-1}), under martian conditions, is best related to thermal conductivity, which can best be related to the grain size of surface materials (1). Thermal inertias measured by the Viking IRTM are useful in determining the nature of materials within the upper tens of centimeters of the surface (1,2). Moderate resolution thermal inertias have been mapped for most of the planet (3), and high resolution data have been analyzed for portions of the planet (2,4,5), including the Tharsis (MC-9) and Phoenicis Lacus (MC-17) Quadrangles, examined here (fig. 1). The high resolution IRTM data used here was taken during Northern winter and spring on Mars, in 1977-1978.

The examined quadrangles are dominated by the Tharsis bulge and the Tharsis Montes, but they also include part of Olympus Mons, and the western end of Valles Marineris, Noctis Labyrinthus. Geologically the area contains some of the youngest rock units on the planet, and comparatively little ancient bedrock (6).

The regional characteristics seen in moderate resolution (3) thermal mapping were seen also in the high resolution data. The area is dominated by low thermal inertias [I<4] over most of the Tharsis region, with some higher inertias [4<I<14] showing up in the canyon area and in the southern plains. For the most part, the low-inertia region in Tharsis is covered by fine paricles (dust) to a depth of several centimeters to a meter (3,7), with a low block abundance (8).

High resolution thermal inertia data was compared with Mars Consortium data, as well. An inverse relationship between albedo and thermal inertia was apparent, as seen on other areas of the planet (2). There was no obvious correlation with elevation, except that elevations higher than 10 km (the large volcanic shields) all showed low inertias. Thermal inertia data was also compared with the geologic units (fig. 2), and no consistent correlation was found. Overall, the inertias were low for the region, regardless of geologic structure or age. An example of this is the Nplc unit (fig. 3), which shows low inertia in MC-17, but showed high inertias in MC-15/23 (2). It is clear that geology does not necessarily control thermal inertia. However, surface albedo is significant, and because albedo features tend to have an aeolian origin (9), thermal inertia information can be related to aeolian deposits.

The purpose of using high resolution data is to look closely at specific geomorphic features and observe their thermal properties. In Tharsis, the volcanoes are especially significant. It was found that there are problems with using high resolution IRTM on the large shield volcanoes. The first involves the temperature-shift corrections, used to compensate for suspended particulates in the atmosphere. It was found that the Tharsis bulge, and each large shield volcano, changes the necessary corrections. It seems that the

lack of a quantitative measure of the amount of particulates in the atmosphere as a function of surface elevation contributes to this effect. Another problem with the volcanoes involves the elevation correction, necessary to compensate for low atmospheric pressures at high elevations. Mars Consortium elevations were used, but it is now clear that Consortium elevations for the large shields are in error as much as 10 km (Table I)(10).

Zimbelman (5) has examined the thermal inertias for the summit of Ascraeus Mons, and has shown that the inertias are virtually the same as for the surrounding plains. It is suggested here that similar results would be found for the other large shields, but the data are less well constrained for those mountains.

Noctis Labyrinthus shows low inertias in the western end, increasing toward the east. Inertias increase inward from the plains to the canyon floor, as found throughout Valles Marineris (4). This likely indicates an average grain size for floor material of medium/coarse sand. The highest inertia in the canyon floor here corresponds with a very low albedo feature.

The rough terrain of the Olympus Aureole (11) and the Cerraunius Fossae showed low, variable inertias. The variation may be related to the way aeolian material may be distributed in this rugged terrain.

The most intriguing thermal feature in the Tharsis area is the Oti Fossae, a fractured zone on the southeast flank of Arsia Mons, which has a seemingly high albedo compared with its surroundings. The area shows high thermal inertias, up to 8, while the surrounding areas are all <4. This area is cooler than the surroundings during the day, and warmer at night (12), so it does not result from internal heat. The inertias are too low to suggest exposed bedrock (1,13), but may be indicative of an exposed or nearly exposed duricrust layer (6). Wind patterns in the area have been studied (10), but it is unclear if there is a wind component sufficient enough to expose duricrust in this area.

The lower-albedo southern plains in this area showed higher inertias, and some aeolian distribution patterns can be seen. For example, a dark patch of material on the west side of a small rise (lat. -26.5, lon. 122.7), has distincly higher thermal inertia than its surroundings.

Overall, the thermal inertias in the Tharsis/Phoenicis Lacus area are low, corresponding with the higher albedo in the Tharsis area. The four large shields present special problems with high-resolution IRTM, but these volcanoes should be looked at individually in more detail. The Noctis Labyrinthus area needs to be related with results covering the rest of the Valles Marineris system (4). In addition, the Oti Fossae should be looked at in more detail. One problem with this is that the Viking photographic coverage of this feature is not good enough to show features which might explain the higher inertia there.

****

1. Kieffer, H. H. et al. (1977) J. Geophys. Res.,82,4249-4291.
2. Zimbelman, J. R., and Leshin, L. A. (1986) submitted to Proc. L.P.S.C. 17.
3. Zimbelman, J. R., and Kieffer, H. H. (1979) J. Geophys. Res.,84,8239-8251.
4. Skinner, S. (1986) [this volume].
5. Zimbelman, J. R. (1986) NASA T. M. #88784,271-572.

6. Scott, D. H., and Carr, M. H. (1978) U.S. Geol. Survey Map I-1083.
7. Jakosky, B.M., and Christensen,P.R. (1986) J. Geophys. Res.,91,3547-3559.
8. Christensen, P. R. (1982) J. Geophys. Res.,87,9985-9998.
9. Veverka, J. et al. (1977) J. Geophys. Res.,82,4167-4187.
10. Lee, S. W. et al. (1982) J. Geophys. Res.,87,10025-10041.
11. Morris, E. C. (1982) J. Geophys. Res.,87,1164-1178.
12. Keiffer, H. H. et al. (1976) Science,194,1346-1351.
13. Zimbelman, J. R. (1986) submitted to Icarus.

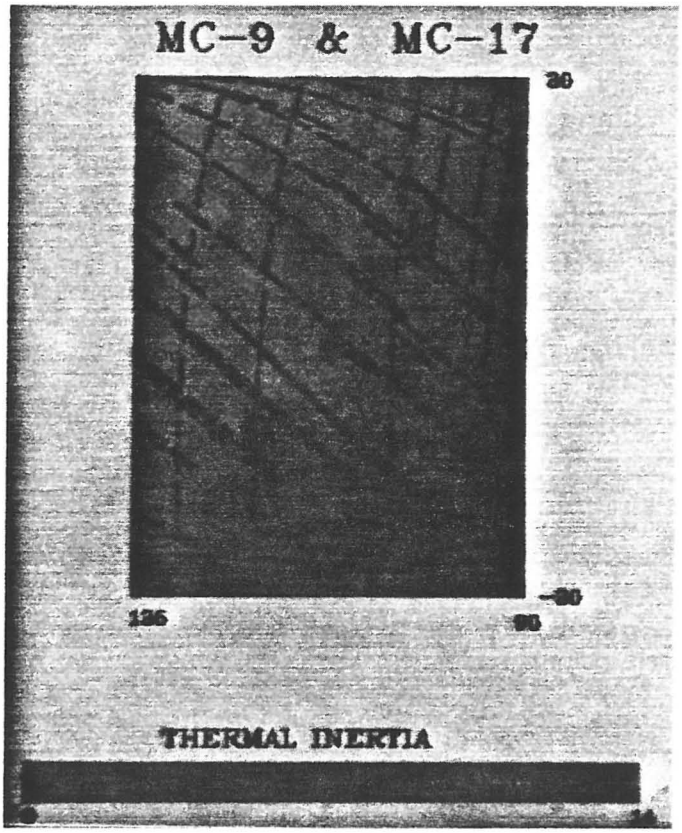

Figure 1: High resolution thermal inertias for Tharsis and Phoenicis Lacus Quadrangles. Data correspond to Viking orbiter groundtracks. The four, circular dark spots are the large volcanic shields.

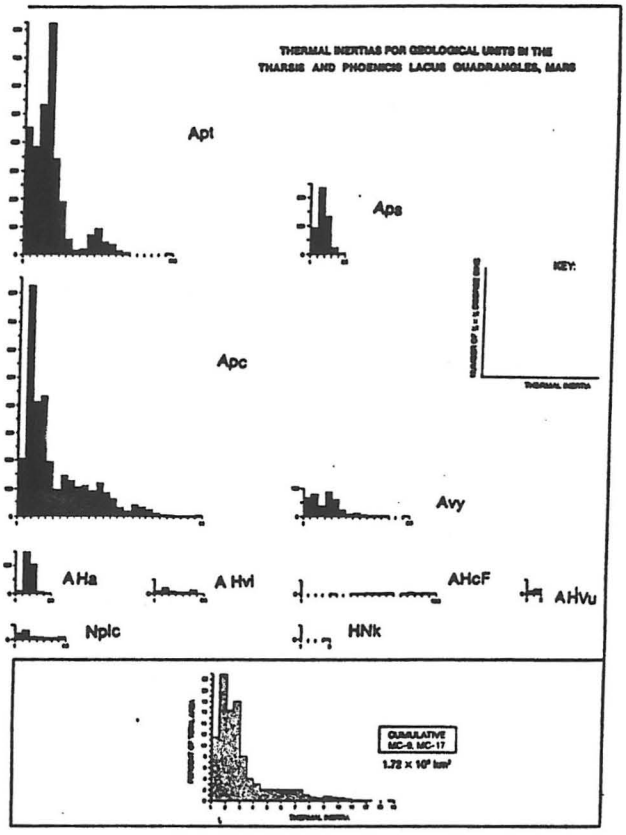

Figure 2

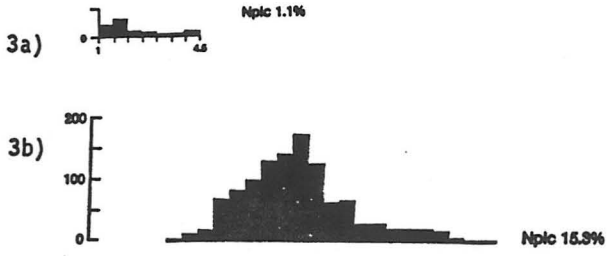

Figure 3: a) Nplc unit thermal inertias in MC-17
b) Nplc unit thermal inertias in MC-15/23

Table I:

	Volcano Elevations (above datum)	
name:	1981 USGS Preliminary:	Mars Consortium/Mariner 9:
Olympus	22-23 km	26-27 km
Ascraeus	22-23 km	27-28 km
Pavonis	17-18 km	27-28 km
Arsia	22-23 km	27-28 km

A GEOCHEMICAL ANALYSIS OF THE RIVER VALLEY ANORTHOSITES, GRENVILLE PROVINCE, ONTARIO; E. A. Eide, Lunar and Planetary Institute Summer Intern Research

The River Valley anorthosite complex of the Grenville Province, Ontario, is an unusual suite relative to all other Proterozoic anorthosites found within the eastern Canadian Shield. Whereas most of the anorthosites from this region were emplaced 1.4-1.7 Ga ago (Emslie, 1985), Sm-Nd isotopic data for the River Valley sequence indicates emplacement at 2.4 Ga (Ashwal, unpublished data). The River Valley anorthosites are also more calcic than their younger Proterozoic counterparts; those of the River Valley contain An_{65-70}, whereas the others contain An_{45-60} (Ashwal, 1982). The complex is located along the Grenville Front, a major reverse fault zone associated with the Grenville Orogeny, which occurred at approximately 1.10-1.15 Ga (Davidson, 1984) and metamorphosed many of the rocks in the Grenville Province, including those in the River Valley area. This study characterizes the geochemistry of this unique anorthosite complex and compares the findings to published data for both older and younger anorthosite suites. Attempts were also made to determine the effects of metamorphism on the rare earth element (REE) content of an anorthosite body.

The samples from the complex range from anorthositic gabbronorites (ca. 70% modal plagioclase) through metagabbros (ca. 20% modal plagioclase). Minor ultramafic rocks are also present. 28 samples from the River Valley complex were analyzed for trace element chemistry using x-ray fluorescence spectroscopy. This technique is also being used to determine major element concentrations. 17 of these 28 were also analyzed for REE and other trace elements using instrumental neutron activation analysis (INAA). Three mineral separates (pyroxene and plagioclase from one rock, and plagioclase from another) were also included for INAA. These data, when normalized to chondritic abundance (Haskin et al, 1968), are used to characterize the complex, evaluate the REE characteristics of the parental liquid for this suite, and compare to other anorthosite types.

The trace element compositions of the samples indicate that a majority have Ni contents between 20 and 100 ppm. The mafic and ultramafic samples have much higher concentrations of Ni (235, 411, and 687 ppm). Yttrium contents vary from 2 to 14 ppm for all samples. Rb and Sr data are consistently low for the mafic and ultramafic rocks (Rb=1-2 ppm; Sr=18-187 ppm) compared to the averages for the rest of the suite (Rb= 2-10 ppm; Sr=230-350 ppm). Samples containing high Zr (41-107 ppm) relative to the whole complex include the mafic-ultramafics and two samples containing large amounts of plagioclase with virtual absence of pyroxene.

The REE patterns for both igneous-textured and recrystallized samples have positive Eu anomalies, consistent with their relatively high modal plagioclase. Both sets of samples are also enriched in LREE (2-6x chondrites) and either flat or depleted HREE (1-5x chondrites). The pyroxene separate and the ultramafic sample have negative Eu anomalies (pyroxene is 3x for LREE and 8x for HREE; ultramafic is 20-30x for LREE and 5-15x for HREE). The data from pyroxene and plagioclase separates were used to calculate the REE pattern for a possible parent magma (distribution coefficients from McKay, Wagstaff, and Yang, 1986). The results show considerable scatter, but in general are consistent with a parent magma with LREE about 60x chondrites. Possible reasons for the imperfect results of these calculations are: 1) difficulties with K_D values, 2) the effects of trapped liquid, and 3) purity of the mineral separates. If perfect adcumulus growth is assumed, however, LREE patterns place the rocks in equilibrium with a melt of 60x chondrites. A liquid of this composition might resemble a continental tholeiite, and

would be an appropriate approximation of a parent magma for most massif anorthosites (Emslie , 1985). Figure 1 represents REE patterns for typical anorthosites from four distinct geologic periods. It correlates increasing An content and REE abundances with the average emplacement ages determined for the samples.

Samples with igneous textures display REE patterns appropriate for cumulate rocks. Mafic mineral content correlates positively with trivalent REE levels, indicating that the rocks are mixtures of cumulus plagioclase and a mafic component--either cumulate pyroxene or trapped liquid, or both. Four of the six recrystallized samples have patterns similar to those with igneous textures, possibly indicating that metamorphism did not modify their REE contents substantially. Two samples, however, each with 65-70% modal plagioclase, have very small positive Eu anomalies, LREE of 20-30x chondrites, and HREE of 3.5-4x chondrites. The LREE ranges are simlar to those of the ultramafic sample. These two anomalous samples have high Zr contents--51 and 41 ppm--and are comparable to 56 ppm found in the ultramafic rock. The high Zr and REE levels in these rocks could indicate the presence of minor amounts of zircon, but it is not certain whether this is a primary feature, or one caused by metamorphic-metasomatic processes.

Conclusions

1) Because the REE patterns of these anorthosites typically show an increase in REE abundances with an increase in mafic content, the rocks are likely to be mixtures of cumulate plagioclase and a mafic component--either cumulate pyroxene or trapped liquid.

2) Generally, the metamorphism of most samples analyzed does not appear to have affected their REE abundances, except in the two cases where zircon may have been introduced into the rock, possibly during a metamorphic or metasomatic event.

3) A calculated parent magma with LREE=60x chondrites for this suite may be representative of a fractionated basalt. Typical MORBs, for example, do not reach more than 10x chondrites. A fractionated basaltic parent supports the two stage crystallization model for anorthosite generation (Emslie, 1985). This model states that plagioclase fractionated from large volumes of basaltic magma at the base of the crust; gravitational settling acted on the mafic components, while the plagioclase crystals formed a crystal "mush" at the top of the chamber, to be intruded later into the upper crust as anorthosites.

4) The geochemistry of River Valley anorthositic rocks is intermediate between Archean (An_{80-95}) (Ashwal, Morrison, Phinney, Wood, 1983) and typical Proterozoic anorthosites (Figure 1). An content for lunar anorthosites is An_{95-97} (Taylor, 1982). It is interesting to consider the significance of a nearly linear relationship between age and many geochemical parameters, including An content and REE abundances, for these distinct anorthosite bodies.

References

Ashwal LD (1982) Proterozoic Anorthosite Massifs: A Review. In: McCallum IS, Walker D (eds) Workshop on Magmatic Processes of Early Planetary Crusts: Magma Oceans and Stratiform Layered Intrusions. LPI Tech, Rpt. 82-01 Lunar and Planetary Institute, Houston, p 40

Ashwal LD, Morrison DA, Phinney WC, Wood J (1983) Origin of Archean Anorthosites: Evidence from the Bad Vermilion Lake Anorthosite Complex, Ontario. Contrib Mineral Petrol 82: 259

Davidson A (1984) Tectonic Boundaries within the Grenville Province of the Canadian Shield. Journal of Geodynamics 1, p 434

Emslie RF (1985) Proterozoic Anorthosite Massifs. In: Tobi AC, Touret JLR (eds) The Deep Proterozoic Crust in the North Atlantic Provinces, p 39.

Haskin LA, Haskin MA, Frey FA, Wildeman TR (1968) Relative and Absolute Terrestrial Abundances of the Rare Earths. In: Ahrens LH (ed) Origin and Distribution of the Elements, p 889-912

McKay G, Wagstaff J, Yang SR (1986) Clinopyroxene REE Distribution Coefficients for Shergottites: The REE content of the Shergotty melt. Geochem Cosmochem Acta 50: 932

Taylor SR (1982) Planetary Science: A Lunar Perspective. The Lunar and Planetary Institute, Houston, p 208

FIG. 1

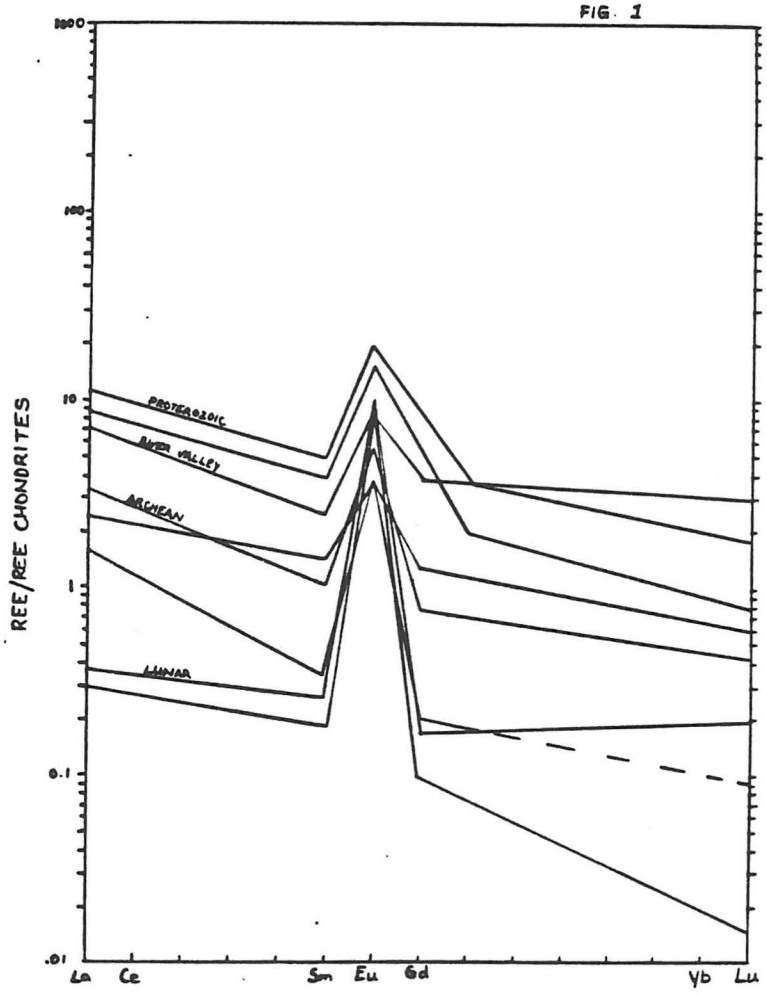

A COMPARISON OF PLUME ERUPTIONS ON IO WITH EARLY LUNAR VOLCANIC PLUME ERUPTIONS

Elizabeth Harding, Rice University, Houston TX and David McKay, NASA Johnson Space Center, Houston TX (advisor)

Volcanic activity was detected on Io in 1979 when Voyager 1 returned several photographs of active plumes to Earth. Several interesting papers proposing plume mechanisms and crustal models for Io soon followed (Smith, et al., 1979; Consolmagno, 1979; Hapke, 1979). All of these models involved sulphur rich crusts and sulphur or SO_2 volcanism. Since 1979, the sulphur dominated crustal models have largely been replaced by hybrid sulphur and silicate models (Carr, 1986) and even (nearly) sulphur free models (Young, 1984).

Lunar igneous rocks were collected by the Apollo 11 astronauts in 1969. Until the mid 1970's, evidence for pyroclastic activity was not generally believed to be present on the Moon. Deposits of small glassy particles collected by the Apollo 15 and 17 missions were often explained in terms of other processes, for example meteor impacts (Roedder and Weiblen, 1973). It is now relatively well established that the sub-millimeter spherule rich deposits explored by Apollos 15 and 17, as well as the "dark mantle deposits" blanketing parts of the Moon, were deposited in lunar pyroclastic eruptions (McGetchin and Head, 1973; Heiken, et al., 1974).

Eruption styles on Io and on the Moon may be more closely related than has generally been thought. Some similarities can readily be noted in Table 1. Among these are plume height, width, and calculated ejection velocities. One problem with comparing these eruption styles is that we have different types of data for each body: we know the composition of the magmatic phase in lunar plumes, but little is known about the gas phase (Wilson and Head, 1983). On Io, the composition of the eruption gas is fairly well constrained (S_2 or SO_2, Smith, 1979; Hapke, 1979; Carr, 1986) but the that of erupting magma (if any is erupted at all) is unknown (Kieffer, 1982). If it can be shown that silicates are ejected in Io plume eruptions and that sulphur gases were important in lunar eruptions, then both Ionian and lunar plumes must be quite similar in composition, consisting of silicate magmas driven by sulphur rich vapors.

The possibility of silicate pyroclastic volcanism on Io has been ignored by most workers. Even in crust models in which the heat sources for plumes are proposed to be silicate magmas at depth (Carr, 1986; Young, 1984) silicate magmas are not considered as possible ejecta. Kieffer (1982) states that if a silicate magma is a heat source for an eruption, some magma could be expected in the plume. At this time, silicate magmatism in the plumes can only be postulated; no silicates have been detected near Io, and IR temperature data can neither prove nor disprove the existence of hot silicate magma in a plume (Carr, 1986).

Sulphur vapor was present in in lunar plumes (Butler and Meyer, 1976; Naughton, et al., 1972). It was the most common condensate found on lunar pyroclastic spherules by Butler and Meyer (1976) and by Grant and his associates (1974). Using a JEOL 35-CF SEM-EDX system equipped with a thin window detector, we analyzed surface condensates on several spherules from Apollo soil sample 74002. We, too, noted that S was the most abundant element. Interestingly, Na was frequently associated with S. Oxygen was not associated with these Na and S rich areas. It is possible that these features are composed of sodium polysulphides (Na_2S, Na_4S_2, or Na_5S_2). These have never before been known to occur naturally, though they have been produced in reactions between liquid sulphur and Na silicate glasses (Hunter and Ingram, 1986).

Na and K are identified in Io's torus, in fact they are the only elements identified there besides S and O. These elements appear to come from Io or its atmosphere (Goldberg, et al., 1984) and it is likely that they are common in Ionian plume vapors (Hapke, 1979). Abundance of Na and K in the vapor phase may be a yet another characteristic common to both Ionian and lunar plume eruptions.

TABLE 1: A Comparison Chart for Ionian and Lunar Plumes.

	Io	Moon
Diameter	3,636 km (1)	3,476 km (1)
Density	3.53 g/cc (1)	3.34 g/cc (1)
Plume height	60 - 300 km (2)	50 - 600 km (8)
Initial velocity	500 - 1000 m/s (2)	100 - 500 m/s (8)
Lateral ejection limit	95 - 600 km (2)	≤ 200 km (8)
Flight time	1000 s (2)	250 s (8*)
Vent diameter	10 m (3)	≤ 10 m (8)
Particle diameter	0.01 μm to 1 mm (4)	10 μm to a few mm (8, 9)
Gas composition	S_2 (6) SO_2 (5) combination (7)	CO (8) $CO+S_2$ + halides (10, 11)
Solid and liquid composition	Solid S_2, SO_2 (5, 6) entrained vent material (4) possible silicate magma (6)	basaltic magma spheres (12, 9)
Gas mass ratio	about 1 (3)	$\leq 10^{-5}$ (8*)

BIBLIOGRAPHY

Butler, P., and Meyer, C., Sulfur Prevails in Coatings on Glass Droplets: Apollo 15 Green and Brown Glasses and Apollo 17 Orange and Black (devitrified) Glasses, *Proc. Lunar Sci Conf. 7th*, 1561-1581, 1976.

Carr, M. H., Silicate Volcanism on Io, *J. Geoph. Res.*, 91, 3521-3532, 1986.

Chapman, C., Matson, D., Newburn, R., Orton, G., Scott, E., Zeller, B., Solar System Fact Finder, Lunar and Planetary Inst. Contr. No. 393, 1979.

Collins, S. A., Spatial Color Variations in the Volcanic Plume at Loki, on Io, *J. Geoph. Res.*, 86, 8621-8626, 1981.

Consolmagno, G., Sulfur Volcanoes on Io (Abstract), *Science*, 205, 397-398, 1979.

Goldberg, R. H., Tombrello, T. A., Burnett, D. S., Fluorine as a Constituent in Lunar Magmatic Gases, *Proc. Lunar Sci. Conf. 7th*, 1597-1613, 1976.

Goldberg, B. A., Garneau, G. W., LaVoie, S. K., Io's Sodium Cloud, *Science*, 226, 512-516, 1984.

Grant, R. W., Housely, R. M., Szalkowski, F. J., Marcus, H. L., Auger Electron Spectroscopy of Lunar Samples, *Proc. Lunar Sci. Conf. 5th*, pp. 2423-2439, 1974.

Hapke, B., Io's Surface and Environs: a Magmatic-Volatile Model, *Geophys. Res. Letters*, 6, 799-802, 1979.

Heiken, G. W., McKay, D. S., Brown, R. W., Lunar Deposits of Possible Pyroclastic Origin, *Geochim et Cosmochim Acta*, 38, 1703-1718, 1974.

Hunter, C. C. and Ingram, M. D., Reactions of Na Ion Conducting Glasses with Molten Sulphur, *Physics and Chemistry of Glasses*, 27, 51-54, 1986.

Kieffer, S. W., Dynamics and Thermodynamics of Volcanic Eruptions: Implications for Plumes on Io, in *Satellites of Jupiter*, edited by D. Morrison, pp. 647-723, Univ. Ariz. Press, 1982.

McGetchin, T. R., and Head, J. W., Lunar Cinder Cones, *Science*, 180, 68-70, 1973.

Meyer, C., McKay, D. S., Anderson, D. H., Butler, P., The Source of Sublimates on the Apollo 15 Green and Apollo 17 Orange Glass Samples, *Proc. Lunar Sci. Conf. 6th*, 1673-1699, 1975.

Naughton, J. J., Hammond, D. A., Margolis, S. V., Muenow, D. W., The Nature and Effect of the Volatile Cloud Produced by Volcanic and Impact Events on the Moon as Derived from a Terrestrial Volcanic Model, *Proc. Lunar Sci. Conf. 3rd*, pp. 2015-2024, 1972.

Roedder, E. and Weiblen, P. W., Origin of Orange Glass Spherules in Apollo 17 Sample 74220, *Trans. of the A. G. U.*, 54, 612-613, 1973.

Smith, B. A., Shoemaker, E. M., Kieffer, S. W., Cook, A. F., The Role of SO_2 in Volcanism on Io, *Nature*, 280, 738-743, 1979.

Strom, R. G. and Schneider, N. M., Volcanic Eruption Plumes on Io, in *Satellites of Jupiter*, edited by D. Morrison, pp. 598-633, Univ. Ariz. Press, 1982.

Strom, R. G., Schneider, N. M., Terrile, R. J., Cook, A. F., Hansen, C., Volcanic Eruptions on Io, J. Geoph. Res., 86, 8593-8620, 1981.

Wilson, L., and Head, J. W., A Comparison of Volcanic Eruption Processes on Earth, Moon, Mars, Io, and Venus, *Nature*, 302, 663-669, 1983.

Wilson, L., and Head, J. W., Ascent and Eruption of Basaltic Magma on the Earth and Moon, *J. Geophys. Res.*, 86,2971-3001, 1981.

Young, Andrew T., No Sulphur Flows on Io, *Icarus*, 58, 197-226,1984.

TABLE REFERENCES

1. Chapman, et al., 1979.
2. Strom and Schneider, 1982.
3. Kieffer, 1982.
4. Collins, 1981.
5. Smith, et al., 1979.
6. Hapke, 1979.
7. Strom, et al., 1981.
8. Wilson and Head, 1981.
9. Heiken, et al., 1974.
10. Goldberg, et al., 1976.
11. Naughton, et al., 1972.
12. Meyer, et al., 1975.

* indicates result calculated from indicated paper.

THE VISCO-ELASTIC RESPONSE OF THE EARTH TO LONG TERM SURFACE LOADS

MODELS OF LAKE BONNEVILLE

by
Grant Marshall
University of California
Santa Cruz

with
Bruce Bills
Lunar and Planetary Institute
8/6/86

To understand more fully the processes by which the earth evolves and changes through time, the mechanical properties of the mantle lithosphere system must be determined for both short and long time scales. For short time scales, both the lithosphere and the mantle appear to respond to applied stresses as elastic bodies; however, for long time scales, the mantle seems to respond as a viscous fluid. The mantle lithosphere system will be discussed here with its application to the Lake Bonneville rebound problem.

Since the subsurface rocks and their environment are not directly accessible, indirect methods of study must be employed in an attempt to determine their properties. With the advent of seismographs, geophysicists have been able to study the seismic waves that have travelled through the interior of the earth. In doing so, many important discoveries have been made about the earths interior, its structure and properties. Seismic waves have a period spectrum ranging from about 1 to 10^4 seconds (2.8 hours). Thus, seismic waves probe the short term response of the interior rocks at relatively high strain rates. To seismic waves, the lithosphere and mantle respond like an elastic solid. Seismic waves can not be used to determine the response of the lithosphere and mantle rocks to long term strains or low strain rates, another method must be employed.

Low strain rates and long term stresses have been applied to the earth from the loads created by glaciers and large lakes. When these large stresses are applied to the earth over long times on the order of 10^4 years or longer, the response of the mantle rocks appears to be that of a viscous fluid while the response of the lithosphere remains elastic. Thus, to accommodate these types of mechanical properties, elastic response to high strain rates and viscous response to low strain rates, a Maxwell visco-elastic model has been applied to the lithosphere upper mantle system. In our treatment of the Lake Bonneville problem we have used Currey's (1982) recent and large data set of the deep lake cycle shoreline measurements to calculate the observed deflection of the lithosphere at the eastern most end of the Basin and Range province in Utah.

At the eastern edge of the Basin and Range province, currently marked by the Wasatch fault zone, a series of Pleistocene lakes have transgressed and regressed periodically filling the interior basin which now is only partially filled by the modern Great Salt Lake of Utah. The largest of the last great lakes was Lake Bonneville which had reached its peak level by ~16.4 kyr BP at 1561 m above sea level with a depth of ~358 m and remained approximately at that level until the great Bonneville flood at ~15.0 kyr BP. After the flood a

new lake level again stablized at about 1450 m; shorelines marking this level are known as the Provo shorelines. At ~14.0 kyr BP the lake again began to drop due to climatic changes and eventually reached a level at which there may have been no water present at ~11.5 kyr BP. The lake again transgressed to a level of 1300 m at ~10.0 kyr BP; this level, being known as the Gilbert shoreline, regressed in 500 yrs to the present level of the Great Salt Lake ~1270 m. On each of the shorelines mentioned, shoreline elevations at points near the center of the basin stand at higher elevations than the corresponding shoreline at the periphery. Thus, the shorelines have recorded a deflection of the lithosphere caused by the surface loading of the lakes and possibly the sediments that have accumulated there. The total maximum deflection for each of the shorelines is: Bonneville, ~76 m; Provo, ~59 m; Gilbert, ~14 m.

To reproduce the observed deflections in the shorelines we have applied a Maxwell visco-elastic model with three variable parameters. The Maxwell visco-elastic model can be thought of schematically as a spring in series with a dashpot filled with a viscous fluid. The lithosphere is considered to be an elastic layer which overlies a visco-elastic channel below which the viscosity is presumed to increase to a higher value. When a constant stress is applied to this model there is an instantaneous initial elastic strain taken up by the spring followed by a slow linearly increasing strain as the dashpot responds to the stress. If an impulsive and exponentially decaying stress is applied, the response is a constant strain. If a sinusoidal stress history is applied then the strain as a function of time will also be sinusiodal; the strain will be in phase with the stress at frequencies below the characteristic frequency (one over the Maxwell time), and it will be out of phase at frequencies above the characteristic frequency. The Maxwell time is defined as the ratio of viscosity to rigidity. The three model parameters that we define are:

1) Lithosphere thickness
2) Effective mantle viscosity
3) Depth of the low viscosity channel.

These three parameters define the three dimensional parameter space which we have searched in an attempt to fit the Lake Bonneville data set. Using a computer model, we have computed the deflection of the lithosphere due to the water load of the great lakes of the Bonneville basin.

The model as described here fits the Bonneville data well. Currey's (1982) data consist of 181 shoreline elevation measurements and dates for the Lake Bonneville shoreline, and 112 measurements for the Provo shoreline, and 48 measurements of the Gilbert shoreline. To map out contours of acceptible models in the parameter space, we have considered only those models which meet the following two test criteria simultaneously:

1) Residual variance not more than a factor of two greater than the best model found
2) Maximum deflection residual not greater than 6 meters.

Using these criteria, we find that there is no one point in the space that fits all three shorelines simultaneously; however, a small area of the space comes very close to fitting all of the shorelines. The values of the parameters in this small area are:

1) Viscosity 10^20 Pa s
2) Lithosphere thickness 24 km
3) Channel depth >400 km.

The model is not sensitive to channel depths greater than 400 km but the acceptible area in parameter space begins to enlarge as smaller depths are used. These values reconstruct 80% of the observed deflection on the Bonneville shoreline. By contouring the residuals we are able observe the spatial orientation of the model's deficiencies. The pattern of the residual contour plot does not appear to be random. There are many areas were the load has been underestimated by only considering the water mass. Our current efforts have focussed on the further investigation of the mass deficiences in the load.

An obvious deficiency of the model is due to its neglect of any load due to sediment in the basin. Several major delta's extend into the basin and their locations can be seen to correlate with the mapped negative residuals from the model. In order to estimate this sediment load we have attempted to model the denudation of the topography due to the many erosional processes that constantly modify topography. Sediment thickness measurements are lacking in most of the area covered by the basin; of the few cores that are available from the region, eight useful values of sediment thickness and age have been obtained, all of which are centered in or near the modern Great Salt Lake. Models of erosion have often been described in terms of a diffusion equation; models of this type have been shown to reproduce erosion modified scarp profiles on the order of 10 m in one dimension. Applying this type of diffusion equation alone to the entire two dimensional Bonneville basin topography array, an area 4 degrees in longitude by 6 degrees in latitude with relief of ~2100 m, leads to unrealistic results in the spatial distribution of the sediment load and is incapable of reproducing the observations. We have proceeded with testing more complicated models in an attempt to recreate the observed sediment measurements.

Currently we are working with an equation that includes three terms. Assuming that the modification of the topography depends on the shape of the topography itself, we have attempted to use an equation that depends on, the elevation of the topography above a specified base level, the local slope of the topography, and the local curvature of the topography. Each of the three terms describe the general macroscopic effect of the many complicated processes by which erosion takes place. The term that depends on the amplitude of the topography above the base level asserts that through time the amplitude of the topography decreases without changing shape. The term that depends on the slope describes the effects of slope degradation, slope failure or mass wasting; steeper slopes tend to erode at a faster rate than more gentle slopes. The last term, which depends on the curvature of the topography, describes the smoothing of the land surface through time; erosion and deposition tend to be more vigorous at points that have a high curvature. With the modeling of the sediment load we hope to be able to explain most of the remaining 20% of the lithospheric deflection in the Lake Bonneville region. Once the full model of sedimentation and flecture is completed we will have a more complete understanding of the dynamics of the lithosphere mantle system in the Basin and Range province in North America.

Currey, D.R. (1982); Lake Bonneville: Selected features of relevance to neotectonic analysis. U.S. Geol. Survey open-file report 82-1070

800 VOLCANOES:
A Census of the Central Andes

Glenn McLaughlin*
Advisors C.A. Wood** and P.W. Francis*
*Lunar and Planetary Institute, Houston, TX 77058
**NASA Johnson Space Center, Houston, TX 77058

More is known of the volcanoes of Mars than of some of Earth's highest volcanoes located within the central Andes Mountains of South America (Francis, 1986). While the Andes' vastness, remoteness and extreme aridity have hampered studies from the ground, these same "problems" make them ideal for scrutiny from space. From a monochrome photo mosaic of Landsat Multispectral Scanner scenes at 1:1 million scale (Bury, 1985), Space Shuttle color photographs and available topographic maps 800 volcanoes have been identified and described, more than twice as many as in any previous compilation. For example, the International Association of Volcanology catalog of post-Miocene volcanoes of the world lists only about 300.

Volcanoes were recognized from space by their symmitry, radial drainage, low albedo, yellow alteration of central slopes and fresh lava. Characteristics noted for each one were name, position summit elevation, edifice height, diameter of cone and crater, diameter of deposits beyond cone and length of the longest lava flow. Volcanoes were also classified by type, the majority being classed as simple composite volcanoes. Resurgent calderas, Mt. St. Helen's-type breached cones and ignimbrite sheets (broad domes of pumiceous pyroclastic flows) were a few other recognized types. Based on the volcanoes state of erosion, a relative geomorphic age was assigned. These ages were five gradations from age 1, for fresh psot-glacial and active volcanoes, to age 5, for volcanic skeletons. A versatile personal computer spreadsheet, Lotus 1-2-3, was employed to store the database of more than 10,000 items and allowed sorting, graphing and statistics to be performed quickly.

The database is a distillation of geomorphic data from many sources and a basic tool for studying regional trends within the diverse Andes' volcanoes. The first figure shows that diversity in its large fields of populations by age 1 (recent), age 3 (mature) and age 5 (very old ~ 20 m.y.) volcanoes. Age 1 volcanoes slump, over time, into age 5 mountains half as high and twice as wide. The small region in the second figure shows the clustering and lineation of volcanoes seen throughout the arc. In most places active volcanoes form a western front; older volcanoes appear further inland, often in parallel rows. Salars are large salt encrusted playas that typically contain no volcanoes. Another sort of large scale struture control are divisions of the arc into nine segments roughly perpendicular to the strike of the arc. (Bury, 1985). Inclusion of geochemical and absolute dates into the database will allow the character and persistence of these segments during the past 20 million years to be examined.

Referrences:

Bury, Andrew (1985) Volcano census of the central Andes, 1985 Summer Intern Conference, Lunar and Planetary Instritute, Houston, p. 16-19.

Francis, P.W. (1986) Volcanology from space; using Landsat Thermatic Mapper data in the central Andes, EOS Tansactions, AGU, Vol 67, No. 14 p. 170-171.

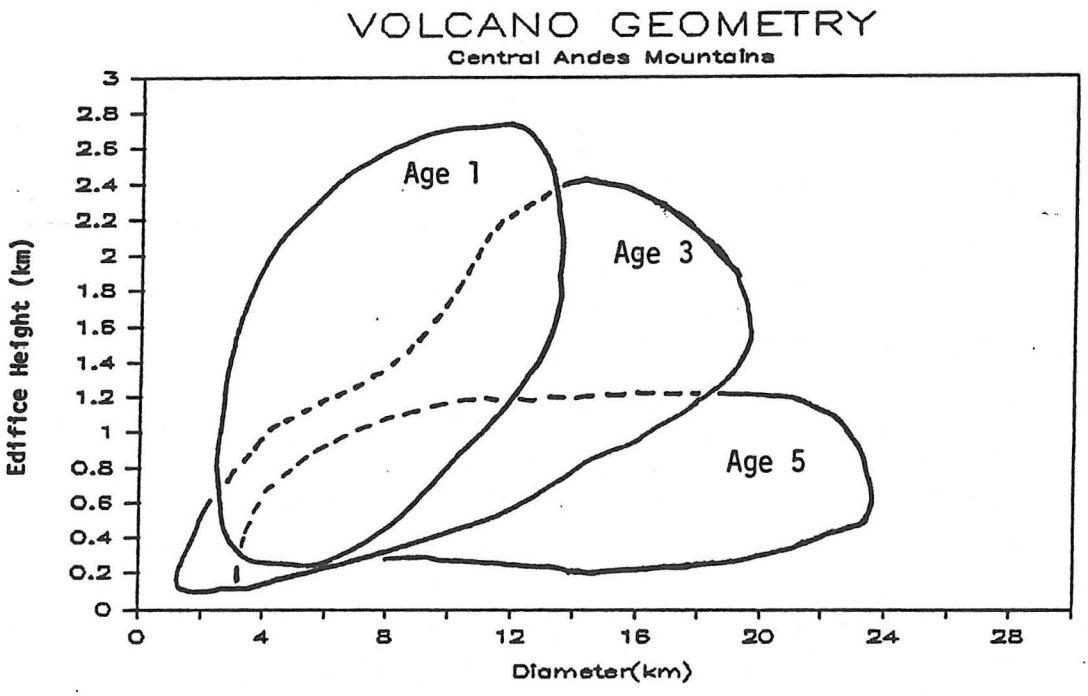

The evolution of Andean volcano shape through time. Age 1's erode into age 2's (not shown), then 3's, 4's and finally short age 5's.

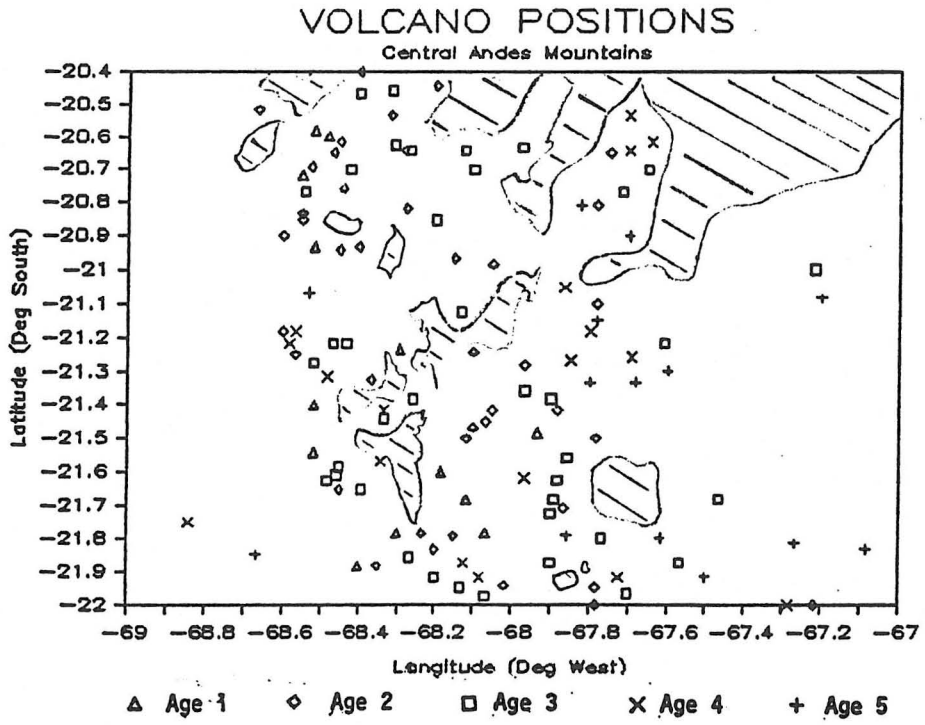

Regional variation of volcano position and age south of Salar de Uyuni.

PHOTOMOSAIC OF VIKING IMAGES 14A29-14A35: A STUDY OF THE GEOMORPHOLOGY OF GANGIS AND CAPRI CHASMAS: David E. Melendrez, Dept. of Geological Sciences, California State Polytechnic University, Pomona 3801 West Temple Ave., Pomona, California 91768-4032, Advisors: Dr. James R. Zimbelman, Dr. Peter W. Francis, Lunar and PLanetary Institute

Valles Marineris is the largest canyon system on the surface of Mars and the largest known in the solar system. One of the smaller sub-canyons running roughly parallel to the main canyon is named Gangis Chasma. It contains a number of large landslides and other expressions of mass wasting. One of the best examples of a geological process on Mars is the largest landslide found within Gangis Chasma, near the junction with Capri Chasma.[1] A process to study this geologically interesting area was carried out involving digital image processing of the original Viking orbiter data, specifically, from Viking orbiter 1 on orbit 14 using frames 29 through 35.

Histograms of each frame were generated by the computer (VAX 11/780) in order to determine the distribution of pixel digital number (DN) values which range from 0 (black) to 255 (white). When a compressed distribution existed, various types of "stretches" (linear and piecewise) were used to enhance surface contrast and add a more uniform brightness to the scene. Bad pixels were replaced by either averaging the pixels' DN values on either side or by simply "patching" the anomalous area with a representative one that was of equal size. Digital filtering also aided in bringing a more uniform brightness to the scene and in enhancing surface details. Control points (coincident pixels from two frames that occur in the area of overlap between those frames) were found in order to geometrically correct the images to ensure a better fit with each other. When the individual frames were joined to form the mosaic, the frames' margins were scarcely noticeable.

These seven frames cover an area from about 42.3°W. long. to about 46.0°W. long. and from about -5.7°S. lat. to about -11.4°S. lat.[2] The oblique orientation of the features is due to the position of the spacecraft at the time the images were recorded. The viewing direction is almost due south (north azimuth $\simeq 179^{0}$ from line of sight) with the emission angle being $\simeq 65^{0}$ from the vertical. The average range of the spacecraft from the surface was 2338.4 kilometers.

Relative age relationships can be determined for a number of features. Several of the large impact craters have been cut away, either partially or almost entirely, by later sliding events along the canyon walls. This implies that those craters are older than the canyon or at least older than the landslides. Some older craters on the plains have been buried by obviously more recent lava flows of fairly low viscosity. Stratigraphy is visible within the canyon walls especially above what appear to be relatively young landslides. The large landslide found in frame 14A30 has exposed an excellent section through an older crater on the adjacent plain. This area of intense mass-wasting activity contains at least three major slides with the largest one being the most recent since it overrides the other two. It also displays classic landslide features including huge slump blocks and a debris flow apron consisting of grooved material. The exposed canyon wall is up to 2 km high and shows little evidence of fluvial

erosion, however, wind erosion may play a role in the formation of fresh talus slopes.[3,4]

Near the area where Gangis Chasma joins Capri Chasma there is a chaotic area displaying intense fluvial erosion. This may have resulted from melting of subsurface ice due to the heat from a rising pool of magma late in the active stage of Tharsis volcanism.[4] This could have led to extensive subsidence of the crust over the slurry of ice and water liberating the liquid water to flow over the surface. The source area would then appear as a hummocky, chaotic terrain adjacent to an area of fluvial erosion and sedimentary structures.

(1) Spitzer, C.R., ed., NASA SP-441, 23, 1980.
(2) Batson, R.M., et.al., NASA SP-438, 58, 1979.
(3) Blasius, K.R., et.al., J. Geophys. Res. 82, 4067-4091, 1977.
(4) Lucchitta, B.K., J. Geophys. Res. 84, 8097-8113, 1979.

Acknowledgement:
The photo in Figure 2. was produced on an Optronics C4300 Colorwrite on loan from the NASA/Johnson Space Center.

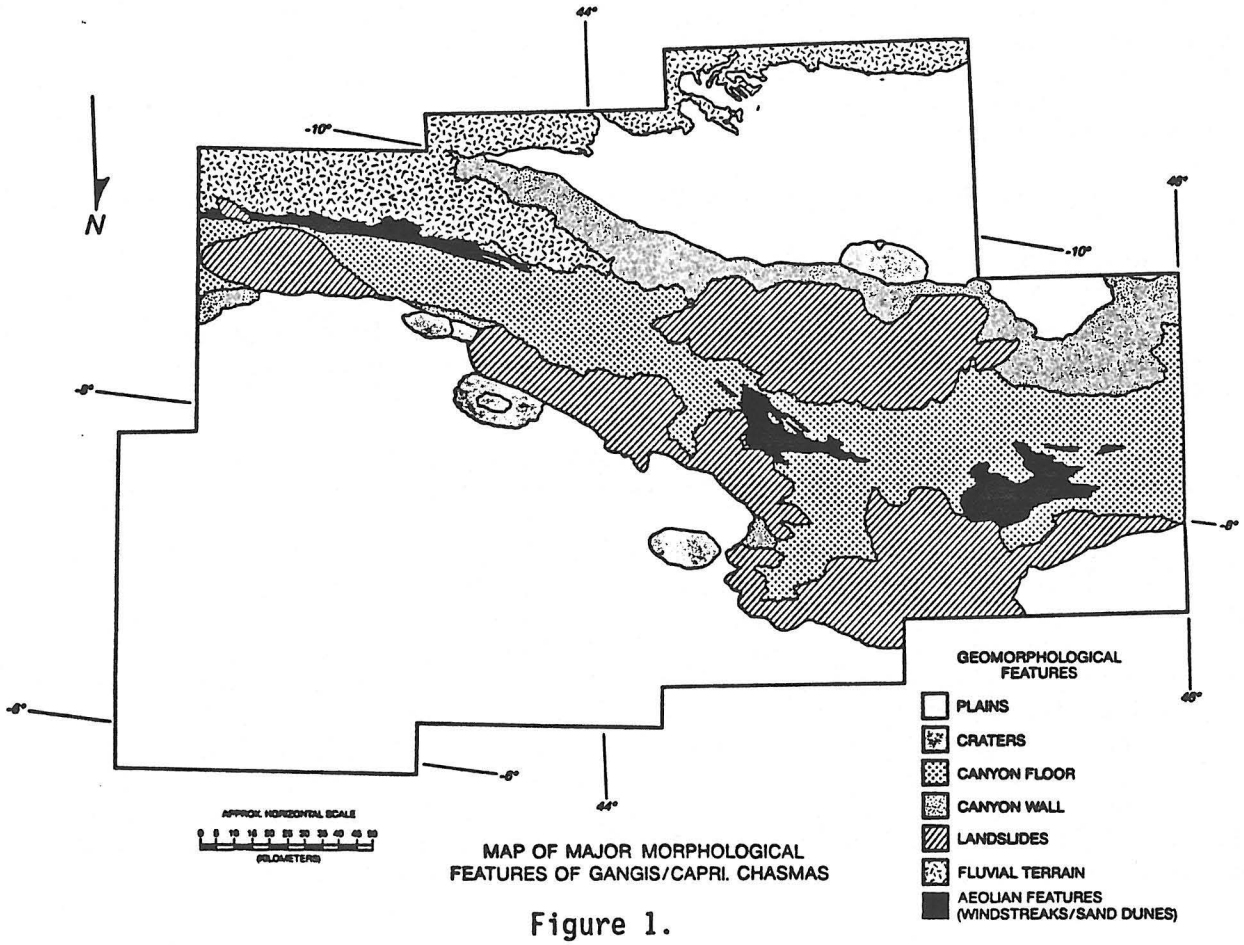

MAP OF MAJOR MORPHOLOGICAL FEATURES OF GANGIS/CAPRI CHASMAS

Figure 1.

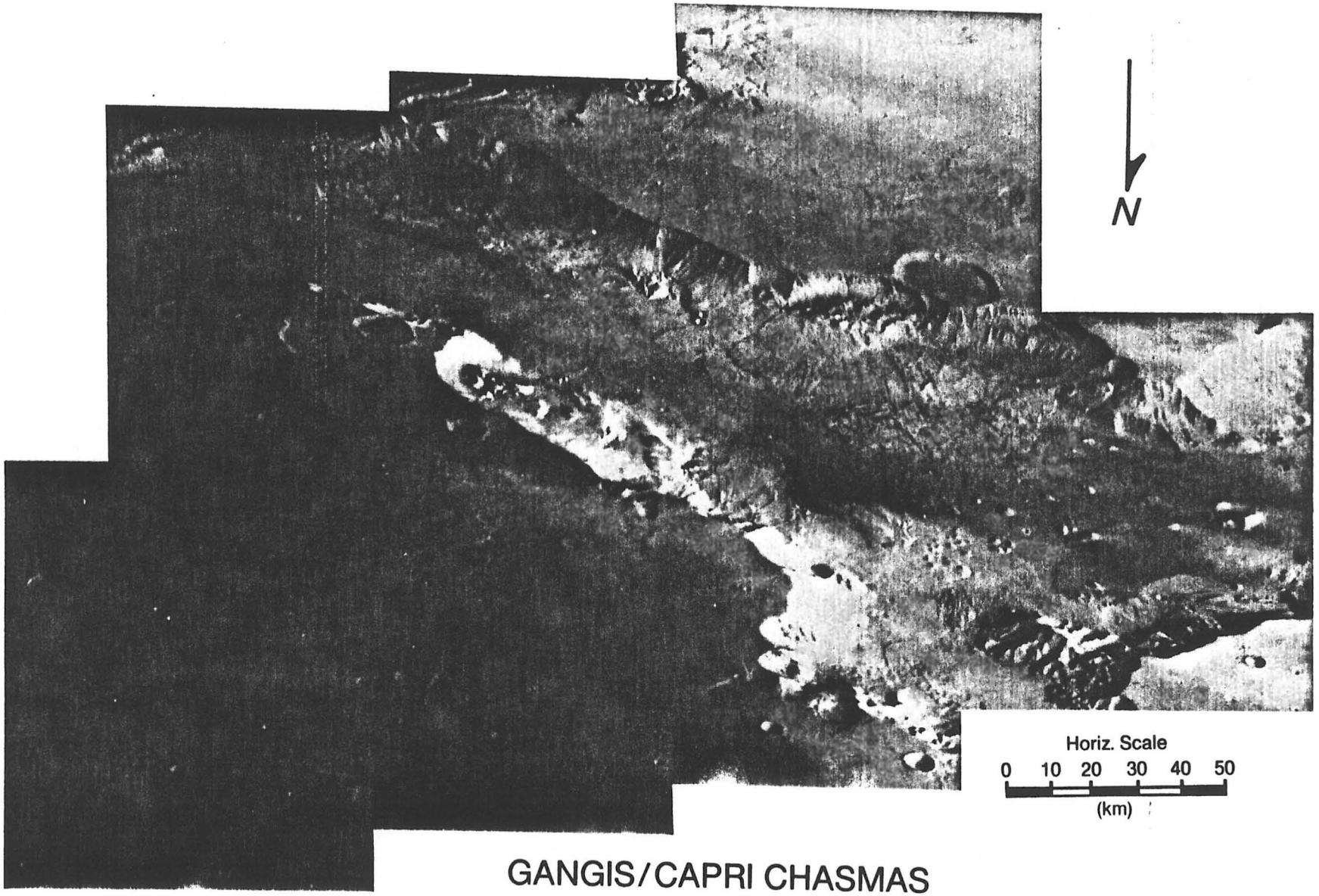

Figure 2.

SHERGOTTY PHOSPHATES: GEOCHEMISTRY OF THE LATE STAGE SHERGOTTY PARENT MELT

Richard J. Nevle, Amherst College Dept. of Geology, L.P.I Summer Intern
Advisor: Dr. Gordon A. McKay, NASA-JSC

Interest in the Shergotty achondrite was renewed when Jagoutz and Wanke (1) reported an internal Sm-Nd isochron for three pyroxene separates, and suggested a 350 my crystallization age for the meteorite, postdating the previously inferred age of 1200 my (2). However, representative points for the whole rock and acid leached phases do not plot on this isochron (1), leading Laul et al. (3) to suggest that Shergotty was subjected to post-magmatic chemical alteration. Furthermore, the wide variation in Sm-Nd ratios led McKay et al. (4) to measure Ce by electron microprobe in order to determine possible contamination of the pyroxenes by an LREE enriched minor phase. McKay et al found that the extreme LREE enrichment reported by (1) was not intrinsic to the pyroxenes. Modeling of Shergotty melts by (4) revealed that measured REE distribution coefficients are inconsistent with the LREE enrichment of the rim pyroxenes reported by (1).

In this study, abundances of major and minor elements in several phosphates of Shergotty and EETA79001 were measured by the electron microprobe. Electron backscatter imaging was used to photograph various phosphate regions to aid in determining local petrography near the phosphate phases. Concentration of REE's in the Shergotty phosphates is presently being measured with the ion probe.

RESULTS

Backscatter photographs reveal that the EETA phosphate inventory is composed of whitlockites, but both whitlockite and apatite are present in Shergotty. It should be noted that two analyses in EETA of points of apatite-like compositions were not confirmed as apatite. Two distinct whitlockite morphologies also reported by (5) emerge as the dominanant mode of occurence in both meteorites. Equant whitlockite crystals are typically adjacent to the Fe-rich rims of pyroxene. Skeletal whitlockite grains are usually surrounded by Fe-rich pyroxene rims, K-rich glass, and maskelynite.

The whitlockites are not chemically zoned, suggesting crystallization under equilibrium conditions. Abundances of Fe, Si, Na, and Mg do not vary between the two whitlockite morphologies. Figures 1 and 2 show the average weight percent composition of Fe, Si, Na, and Mg for both Shergotty and EETA. No extreme variations in chemistry are seen among the whitlockites, except for the average of three analyses from whitlockites in Lithology B of EETA which reveal an Mg/Mg+Fe ratio significantly higher than in any of the whitlockites in Lithology A or Shergotty.

Concentration levels for Yttrium, an analogue for the middle REE's were measured for whitlockites and apatites in Shergotty. Jagoutz and Wanke (2) measured Ce levels in the Shergotty phosphates, pointing out that Ce concentrations varied proportionally to
Mg/Mg+Fe. Furthermore they suggested that the REE abundances were enhanced in the apatites. Comparison of Yttrium to Mg/Mg+Fe does not show a proportionally varying relationship, and Y levels are significantly higher in the whitlockites than in the apatites. Most apatites contained no detectable yttrium, and there is some evidence that whitlockite adjacent to apatite is depleted in yttrium as well. The variation of yttrium atomic concentrations in individual whitlockite analyses are illustrated in Figure 3.

Apatite typically occurs as rims around the whitlockite imlplying that the late stage residual melt was in disequilibrium with respect to whitlockite,

converting it to a more stable apatite phase. One large apatite crystal (400 microns) may have crystallized by a different process, and examination of apatite chemistry continues in order to identify evidence of the conditions of such a process. Many analyses of apatites indicate compositions that are transitional between apatite and whitlockite, which may be simply be indicative of anlyses across phase boundaries. Another possibility is that these intermediate compositions represent a zone of a metastable transitional phase formed as a product of whitlockite alteration.

Another important mode of occurence for apatites is seen in apatite paralleling an iron sulfide vein within a single whitlockite crystal. This observation may be important in terms of the inferences made by (1), who suggested that a contaminating fluid containing Nd altered the original Nd concentration of the meteorite, and hence the Sm-Nd isochron. A late stage or post magmatic Cl-rich fluid may have induced melting of an iron sulfide phase and forced it into the whitlockite converting the adjacent surfaces into apatite. Localized heat produced by the shock event (6) may have also melted the low temperature iron sulfide and apatite and forced the resulting liquid into a whitlockite fracture, but analyses near and of the vein do not show the K and Si enrichment typical of Shergotty shock melt glasses.

CONCLUSION

Clearly, the late stage residual melt of Shergotty was enriched in phosphate phases which represents a phenomenon apparently particular to shergottite meteorites and perhaps of the Martian mantle. The REE patterns of Shergotty are complex and imply that processes other than simple partial melting were neccessary to produce the wide range of Sm-Nd fractionation (4). As the primary reservoirs of REE's in Shergotty, whitlockites may behave as the dominant REE hosts in the Martian mantle, and represent a phase that is more compatible with the Martian LREE's. As seen in Shergotty, the whitlockites crystallized late in parent melt and represent low temperature melting phases. This being the case, whitlockites may be one of the first minerals to be removed during partial melting. Such a process would simultaneously deplete the mantle of LREE's and enrich the evolving daughter magma. When magmas produced by partial melting began to crystallize, incompatible REE's would remain in the liquid phase until whilockite began to appear as a solid phase and REE fractionation into the crystallizing phosphates could proceed. Although major elements apparently do not diffuse into pyroxene from the whitlockite, closer examination of geochemical relationships between whitlockite and pyroxene should continue. Measurements of REE's with the ion probe should be helpful in revealing any chemical trends at the pyroxene-whitlockite phase boundary as well as the geochemical relationships between the Shergotty whitlockites and apatites. The possibility of late stage alteration or post-magmatic chemical alteration of the whitlockites should continue to be considered in future shergottite research to determine whether the crystallizing Shergotty parent
magma became inhomogeneous with respect to its REE inventory. Late stage fluids may have been pathways for REE transportation and disrupted homogeneity of the crystallizing magma with respect to these elements. Post magmatic chemical alteration may have introduced foreign REE's as suggested by (2).

REFERENCES: (1) Jagoutz, E. and Wanke, H. (1986) Geochim. Cosmochim. Acta. 50, 939-954. (2) Shih, et al. (1982) Geochim. Cosmochim. Acta. 46, 2323-2344. (3) Laul, J.C., et al. (1986) Geochim. Cosmochim. Acta. 50, 909-926. (4) McKay, G., et. al. (1986) Geochim. Cosmochim. Acta. 50, 927-938. (5) Treiman, A.H. (1984) Meteoritics 20, 229-243. (6) Lambert, P. (1985) Proc. Meteoritical Soc.

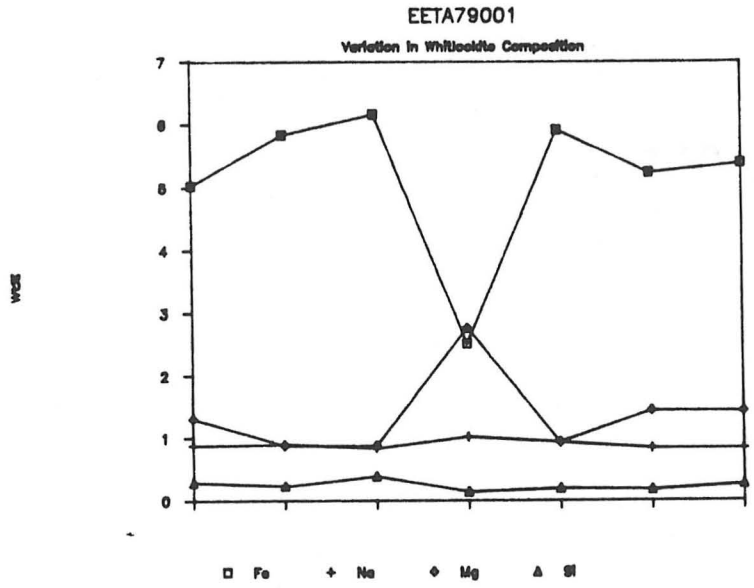

Fig. 1

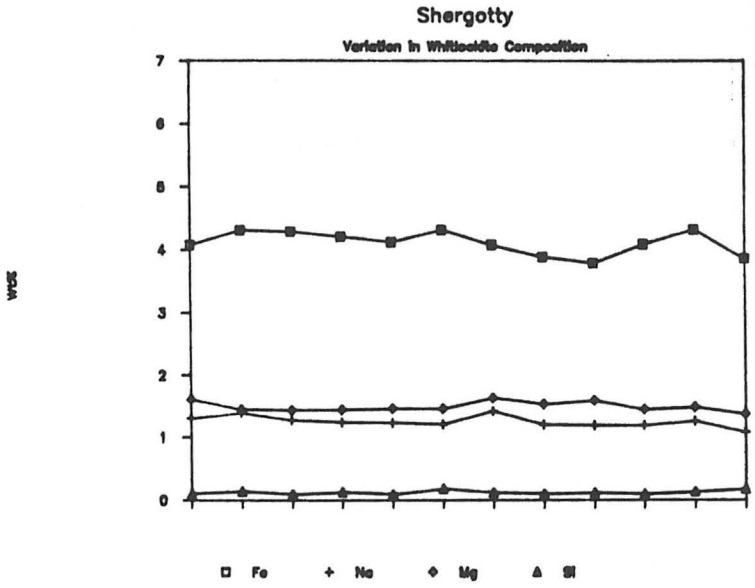

Fig. 2

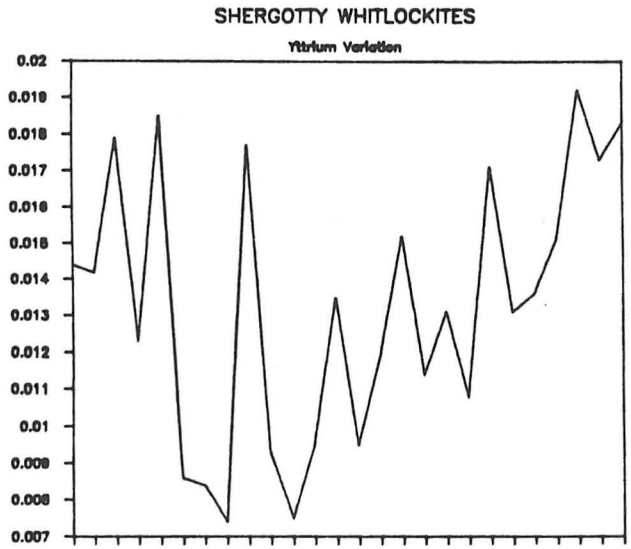

Fig. 3

HYDROGEN ABUNDANCES IN LUNAR SOILS

SIZE AND MINERAL SEPARATES

Anton E. Skaugset, Reed College, Portland Oregon.
Advisor: Dr. Everett K. Gibson Jr.
With the assistance of: Dr. Roberta Bustin
Dr. Rob Carr

In the continuing effort to plan for a lunar base, one of the most persistent problems that researchers face is the acquisition of hydrogen and oxygen, both for use as fuel and for life support. Much work has been done on the reduction of ilmenite to produce oxygen, and it also appears that there is a significant amount of oxygen present in lunar soils and rocks. It would be helpful, however, to have a clear and accurate conception of how much hydrogen is present in lunar materials, and it would also be valuable to have a clearer understanding of the relationships between such easily observable physical parameters as soil composition or maturity and that soil's hydrogen content. This knowledge would certainly be helpful to those who are designing a living environment on the moon, and it was for that reason that a study of hydrogen content in lunar soils was undertaken.

Before any data on hydrogen concentrations in lunar soils can be analyzed, the source of such hydrogen must be considered. The hydrogen present in lunar soil originates in the solar wind, and is implanted in lunar soils as they lie exposed to direct sunlight. Therefore it could be assumed that the greater the length of time a soil is exposed to the solar wind, the greater the hydrogen content of that soil. Further, it could also be expected that particles with a larger surface would also have a greater hydrogen content, if hydrogen is a surface-correlated component.

Data was therefore collected to try and determine the relationship, if any, between particle size and hydrogen concentration. In addition, the relationship between hydrogen content and mineral type was also explored.

The procedure for determining the hydrogen in a soil sample was as follows: The sample under study, (typically ten milligrams or less) was weighed precisely. The sample was then placed in an alumina tube crucible, which was then evacuated. The tube was then heated at 850-900 degrees Celcius for three minutes, and the gases evolved during pyrolysis were injected into a gas chromatograph. The column used was molecular sieve 5A, which yields good resolution of the hydrogen peak. The detector used was a helium ionization detector, which has a very high sensitivity. Any signals corresponding to a hydrogen peak received from the detector were recorded on a chart recorder, and the peaks automatically integrated by a Spectra-Physics SP400 integrator. The areas of the integrated hydrogen peaks were then plotted on a previously prepared calibration curve, the weight fraction hydrogen calculated, and the hydrogen content recorded in parts-per-million.

The results of the study into hydrogen content and particle size are as follows: As particle size decreases, hydrogen content increases. When hydrogen content is plotted against particle size on a log-log graph, the resulting graph is a line that is quite linear for small particle diameter, but assumes an upward concave curve for larger particles. It is assumed that

the initial slope represents the dependance of hydrogen retention on surface area, while in the larger particles, the contribution due to dependance on the volume of the particles, and the individual soil's exposure history, become more important. This correlation has been seen for gases trapped in lunar soils earlier, although the gases analyzed were the solar wind noble gases (ref. Schultz et al.; Proc. Lunar Sci. Conf. Eighth [1977] p. 2799-2815). The distribution pattern for helium in lunar soil size separates has also been shown to apply for distribution of hydrogen in lunar soils, for the same grain sizes.

The study of selected mineral separates was also informative; After agglutinate and ilmenite separates were hand-picked from several size fractions, they were analyzed for hydrogen content in the same manner as the size separates above. The agglutinates were found to be enriched in hydrogen, by a factor as great as ten, relative to the same size fraction of the parent soil. Ilmenites, on the other hand, were often found to be depleted in hydrogen in those soils that contained significant amounts of hydrogen, or, at best, to have values for hydrogen concentration on the same order as the parent soil. The greater abundance of solar wind hydrogen in agglutinate particles is not surprising, due to the structure of the particles themselves. Agglutinates are a product of the micrometeoritic bombardment of the moons surface. They are aggregate clumps of rock fragments and soils, bound together by impact glass, and possessing a relatively low density. Formed as they are in tiny impacts of terrific energy, agglutinates have a cindery appearance, and they have a very large surface area for their individual diameter. It is not surprising, therefore, that agglutinates can trap hydrogen, or at least hold hydrogen, better than an equal weight of bulk soil. The depletion of hydrogen in ilmenite came as a surprise, however. Ilmenite had previously been found to be enriched in solar wind helium (H. Hintenberger, et al.; Proc. Lunar Sci. Conf. Fifth, [1974] pp. 2005-2022). It had been assumed that a similar enrichment would be found for hydrogen, as hydrogen is more abundant in the solar wind than helium. Previous studies in the lab had shown ilmenite to be hydrogen poor, but the method of separation of the mineral had been suspect: These studies, using hand sorted ilmenites, have shown that the hydrogen poverty of ilmenites in lunar soil is a reality.

The experimental method was shown to be accurate, and reproducible. The principle limiting factor in the research done was the limitation on sample size, due to the precious nature of lunar materials. Increasing sample size, or increasing the number ofindividual samples analyzed would undoubtedly enhance experimental accuracy.

MINERAL SEPARATES

HYDROGEN DATA SUMMARY

sample #	Particle size (microns)	"Total" sample (ppm)	Ilmenites (ppm)	Agglutinates (ppm)
71501,138	90-150	7.7	---	22.2
	150-250	2.0	3.8	20.0
	250-500	2.3	3.5	10.2
	500-1000	1.7	1.2	4.7
10084,149	90-150	20.2	---	---
	150-250	11.3	7.0	16.6
	250-500	15.7	4.3	16.8
	500-1000	7.2	3.7	11.5
60501,1	250-500	4.5	2.9	11.4
12070,127	250-500	9.4	3.6	7.4
15021,2	250-500	8.3	---	11.2

HYDROGEN ABUNDANCES IN LUNAR SOILS--SIZE SEPARATES

SOIL:	10084,149	12070,127	15021,2	60501,1	71501,138
GRAIN SIZE (microns)					
500-1000	7.2	8.5	11.0	2.6	1.7
250-500	15.7	9.4	8.3	4.5	2.4
150-250	11.3	7.5	8.4	5.2	2.0
90-150	20.2	8.7	15.5	9.6	7.7
75-90	20.1	9.1	20.8	12.9	9.4
45-75	24.4	16.2	22.4	16.1	18.5
20-45	39.7	30.1	51.1	43.1	47.2
< 20	146.7	107.4	128.5	124.1	126.5
BULK VALUES:					
Calculated:	55.1	35.5	49.8	42.6	35.8
Measured:	54.2	39.2	49.6	35.8	25.7
Is/FeO:	78	47	70	80	35

THERMAL INERTIA DATA OF LUNAE PALUS AND COPRATES QUADRANGLES, MARS

Stephanie Skinner, 1986 summer intern
Department of Earth Sciences, University of Northern Iowa
James Zimbelman, advisor

The Viking infrared thermal mapper, IRTM, produced data of Mars which mapped, in high-resolution, the Lunae Palus and Coprates quadrangles (1, fig 1). The information received, combined with data from low-resolution mapping, aid in the determination of the geological processes working on the planet.

Lunae Palus (0^{o} to 30^{o}N, 45^{o} to 90^{o}W) contains vast lava flow plains which originated west of the quadrangle by the Tharsis volcanoes. The eastern part of the quadrangle contains a much heavier cratered flow plain than the west. Lunae Palus is privileged to contain the location of the Viking 1 Lander site. Directly south of Lunae Palus is the Coprates quadrangle (0^{o} to 30^{o}S, 45^{o} to 90^{o}W). Most of Valles Marineris lies within the Coprates quadrangle. The large canyons are characterized by debris slides, jumbled masses of rock, and sand dunes.

Thermal inertia is the quantitative measurement of surface temperature changes caused by insolating conditions (2). It is the square root of the product of density, specific heat, and thermal conductivity measured in units of 10^{-3} cal cm^{-2} $sec^{-1/2}$ K^{-1} (1). In Lunae Palus and Coprates quadrangles thermal inertia values vary from 1 to greater than 18. Typically, the canyons and channels show very high thermal inertia values as compared to the surrounding plains.

The western and southeastern parts of Lunae Palus, Lunae Planum, is distinguished by lava flow plains. The western half displays thermal inertia values consistently between 1 and 3. Values between 5 and 7 are found in the southeastern region. According to a geologic map by Scott and Carr (3), this area is mostly covered by cratered, volcanic, and ridged plains material. Stratigraphically speaking, the ridged plains are the oldest as determined by crater age relationships. The distribution of the geological units and the thermal inertia trends are not well correlated. Thus implying that some other process is the primary influence in the area. The thermal inertia values suggest that the ground covering on the plains is on the order of silt to very fine grained sand (4).

Directly east of Lunae Planum is Kasei Valles, a very large channel. Unfortunatly, the thermal data through the channel was taken during the afternoon. The Viking Lander 1 verified that this location experiences afternoon cooling. It is the result of a layered soil. The upper layer is a thin covering of dust underlain by duricrust (5,6). The dust layer absorbs heat during the day which is transferred to the duricrust during the early evening and night. As the dust layer cools after sunset, the duricrust emits heat throughout the night and early morning. However, during the afternoon, the duricrust loses the stored heat and thus shows lower thermal inertias than expected during these hours.

The plains south of Valles Marineris have higher thermal inertias than the northern plains. The values correspond to fine sand grain sizes (4). The geologic units are identical to those in the northern plains. The explanation for the difference between the two hemispheres deals with the weather patterns on the planet (7). The southern hemisphere is presently closest to the sun during perihelion. During this close approach, the wind patterns cause the start of the global dust storms. Circular wind patterns trap sand size

particles in these circular areas of the planet. These remaining sand size particles create higher thermal inertia values than the silt size northern deposits.

The canyon system typically displays the highest thermal inertias on the wall and in jumbled chaotic areas. However, the thermal data might be influenced by the sun angle for the daytime tracks. Most of the walls show high thermal inertias, potentially due to bare rock exposure. The spatial resolution was insufficient to distinguish individual layers exposed in the canyon walls. Generally, the high thermal inertia areas in the canyon correspond with low albedo regions (fig 2).

By looking at low range Viking photos layering within the canyon walls can be seen. The layering is observed in the upper hundreds of meters of the wall. The layers are so distinct as one can follow a layer around the canyon wall. The western end of Candor Chasma contains within its wall a layer of about 80 meters. Higher resolution pictures are needed to get a closer view of these layers in order to determine their origin. The layers could extend all of the way to the bottom of the canyons but there they are covered by landslide materials. This would explain the varying thickness of layers in different segments of the canyon walls.

Juventae Chasma (5^{o}S, 60^{o}W) displays much higher thermal inertia than the other canyons. By looking at low range photos, a closer look of the jumbled chaotic terrain is accomplished. The origin of the rock mass is not fully understood. However, it is believed that the unconfined runoff channel in the northern section of the canyon could be the source of the jumbled rock. The beginning point of unconfined channels are typically areas of chaotic terrain (8). These masses of jumbled rock could cause the observed increase in thermal inertia.

Craters found in the southern highlands appear to have higher thermal inertia values than those in the northern plains. These craters have jumbled rock masses along their walls. One crater, located at 17^{o}S 54^{o}W, has a fracture running through it. The fracture and the crater walls all show inertia values in the mid-teens. By looking at low range photos it was determined that the high values are directly due to large blocks of rock.

In order to better understand the geologic processes that have taken and are taking place on Mars, more detailed studies of the planet are necessary. Since infrared data only examines the upper few centimeters of the soil, the determination of the underlying structures could be obtained with the use of a radar telescope on the next Martian orbiter.

REFERENCES

1. Kieffer, H., et al., 1977, J. Geophys. Res., 82, p. 4249-4291.
2. Zimbelman, J., and Leshin, L., 1986, submitted to Proc. 17th LPSC.
3. Scott, D., and Carr, M., 1978, US Geological Survey Map I-1083.
4. Kieffer, H., et al., 1973, J. Geophys. Res., 78, p. 32.
5. Ditteon, R., 1982, J. Geophys. Res., 87, p. 10197-10214.
6. Christensen, P., et al., 1986, NASA TM-88383, p. 515-517.
7. Christensen, P., 1986, J. Geophys. Res., 91, p. 3533-3545.
8. Carr, M., 1982, The Surface of Mars, p. 125.

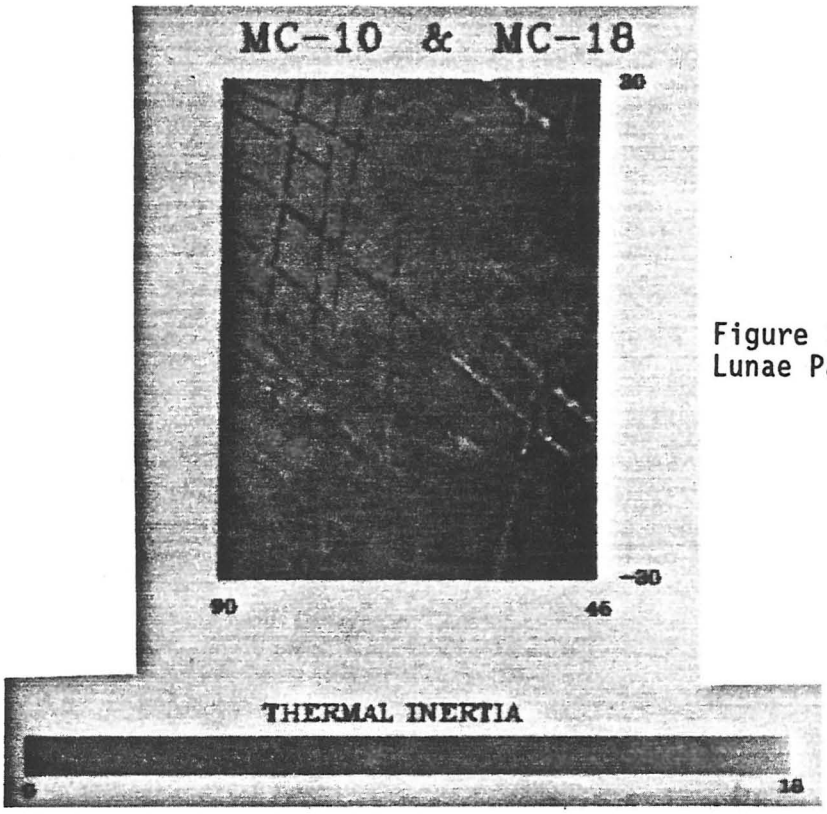

Figure 1: IRTM Data in Lunae Palus and Coprates

Figure 2: Albedo features in Valles Marineris

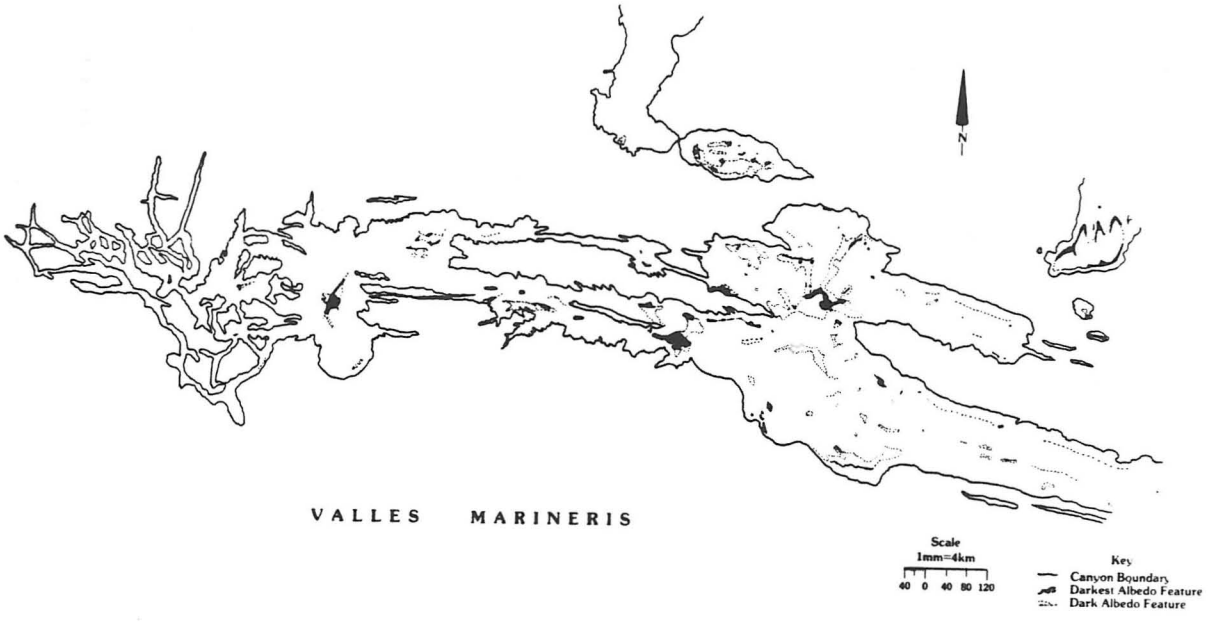

I. THE STILLWATER INTRUSION: A LUNAR ANALOG STUDY

II. AN EXAMINATION OF APOLLO 15 MARE BASALTS

Alison M. Steele, Department of Geology, Acadia University, Wolfville, Nova Scotia, Canada B0P 1X0
Advisor: Dr. Graham Ryder, Lunar and Planetary Institute, Houston, Texas 77058

I. The plutonic rocks of the lunar highlands (4.0-4.4 billion years old) include such types as anorthosite and norite and are crucial for the understanding of the early history of the Moon. However, the study of these rocks and therefore the interpretation of their conditions of formation are hindered by the fact that the samples collected were small random samples, unlike terrestrial samples which are usually collected in a stratigraphic context from a known source. As a result of the more extensive nature of terrestrial studies, no completely suitable framework exists for the interpretation of intensive data from single samples; determinations of parental magmas, for example, are not usually made from single rocks.

As an approach to this problem, a detailed lunar-like study of a more well-known example, the Stillwater Igneous Complex of Montana, was undertaken. The Stillwater Intrusion is a strongly differentiated layered basic intrusion with a stratigraphic thickness of approximately 4.4 km (Raedeke and McCallum, 1984). This intrusion serves as as an excellent lunar analog for the following reasons: it is plutonic, it contains comparable amounts of orthopyroxene and plagioclase, and it also exhibits extensive layers of anorthosite (Ryder and Spettel, 1985).

The samples examined were from the Lower Banded Zone of the Stillwater Intrusion, the section which is characterized by the first appearance of plagioclase as a cumulate phase. Two series of samples were examined. The 8-Series samples were taken from three homogeneous but contrasting layers of a 7.5 m section of the Norite 1 Subzone, and the 3-Series from 4 successive bands in a 10 m interval of the Gabbronorite 1 Subzone. Samples from both series have a simple mineralogy consisting generally of three mineral phases: plagioclase, orthopyroxene, and clinopyroxene. Sample proximity in each series is the basis for the assumption that the rocks crystallized from the same parent magma; in an intrusion over 4 km thick, it is unlikely that new magma pulses would substantially influence such restricted stratigraphic intervals (pulses would probably be volumetrically insignificant and statistically unlikely), if such pulses did occur (Ryder and Spettel, 1985).

Both major elements and Rare Earth elements of the samples were analysed using the following techniques: Instrumental Neutron Activation Analysis of whole rock powders of the 3-Series and mineral separates of both series (excluding the anorthosite of the 8-Series), and X-Ray Fluorescence of the 3-Series whole rocks. Emphasis was placed on the REE because they provide a coherent data set and exhibit similar chemical behavior. The data obtained in this study is complimentary to previous work on both series of rocks in which Electron Microprobe and petrographic studies were done on thin sections of the samples.

Analyses of both mineral separates and whole rock powders were done so that the current model for determining a parental magma composition could be tested. Theoretically, if one assumes that a rock is a perfect adcumulate (i.e. contains no trapped magmatic liquid), all mineral separates and whole rock analyses should yield virtually the same calculated parent magmas.

Possible sources of error could lie with the REE analysis itself, or with the ratios between the REE distribution coefficients which are used in the calculations (these coefficients have not been thoroughly investigated and may or may not be wholly appropriate for this particular analysis). Another source of error could lie with the assumption that the rocks represent perfect adcumulates. It is unlikely that in every case, the pore space between cumulus crystals was completely eliminated while all the liquid contained in the pores was still able to equilibrate with the parent. Thus far, calculations have assumed that no trapped liquid is present in the rocks, so the next task is to recalculate the parental magmas assuming varying amounts of trapped liquid and see if more precise estimates of the parent can be made.

The raw data obtained from the INAA analyses and the preliminary calculations of parent magmas produced somewhat scattered results (see fig. 1). From this study it is obvious that the petrogenetic evolution of cumulate rocks is not completely understood; crystallization processes themselves may not occur exactly as is now believed, and there may still be limitations as to what can be inferred from REE data. And, if parental magmas cannot presently be calculated for series of samples which are known to have crystallized from the same parent magma, it may be difficult to determine lunar parental magmas from single highlands samples. The model is ultimately more complex than that which is presently postulated, and in order for it to be expanded and modified, it will have to incorporate more fully other closely related considerations, such as the relationships between rock petrography and chemistry.

II. An investigation of a collection of fifteen Apollo 15 mare basalt fragments is currently in progress. These samples represent coarse fines collected in rake samples at Apollo 15 Station 9A. The basalts are being analysed by Instrumental Neutron Activation Analysis (primarily for REE) and also by Electron Microprobe (primarily for whole rock chemistry).

The fragments were examined and described using a binocular microscope during INAA preparation. As well, for the Microprobe study, fused beads were made of small quantities of the whole rock powder using the method of Brown (1977). The aim of the study is to determine the nature and number of any differing mare units present and whether or not these correspond to those proposed by Binder (1985).

REFERENCES

Binder, A. (1985). "Apollo 15 Mare Units and Their Petrogenesis", in **Workshop on the Geology and Petrology of the Apollo 15 Landing Site** (G. Ryder and P. Spudis, ed.'s), LPI Technical Report 86-03.

Brown, R.W. (1977). "A Sample Fusion Technique for Whole Rock Analysis with the Electron Microprobe", Geochimica et Cosmochimica Acta, Vol. 41, pp. 435-438.

McCallum, I.S., Raedeke, L.D., and Mathez, E.A. (1980). "Investigations of the Stillwater Complex, Part 1: Stratigraphy and Structure of the Banded Zone", American Journal of Science, Vol. 280-A, pp.59-87.

Ryder, G., and Spettel, B. (1985). "The Parental Magma for Some Rocks from the Norite 1 Subzone of the Stillwater Complex: A Lunar Analog Study", Proceedings of the Fifteenth Lunar and Planetary Science Conference, Part 2, Journal of Geophysical Research, Vol. 90, Supplement, pp. C591-C600.

FIGURE 1
STILLWATER DATA

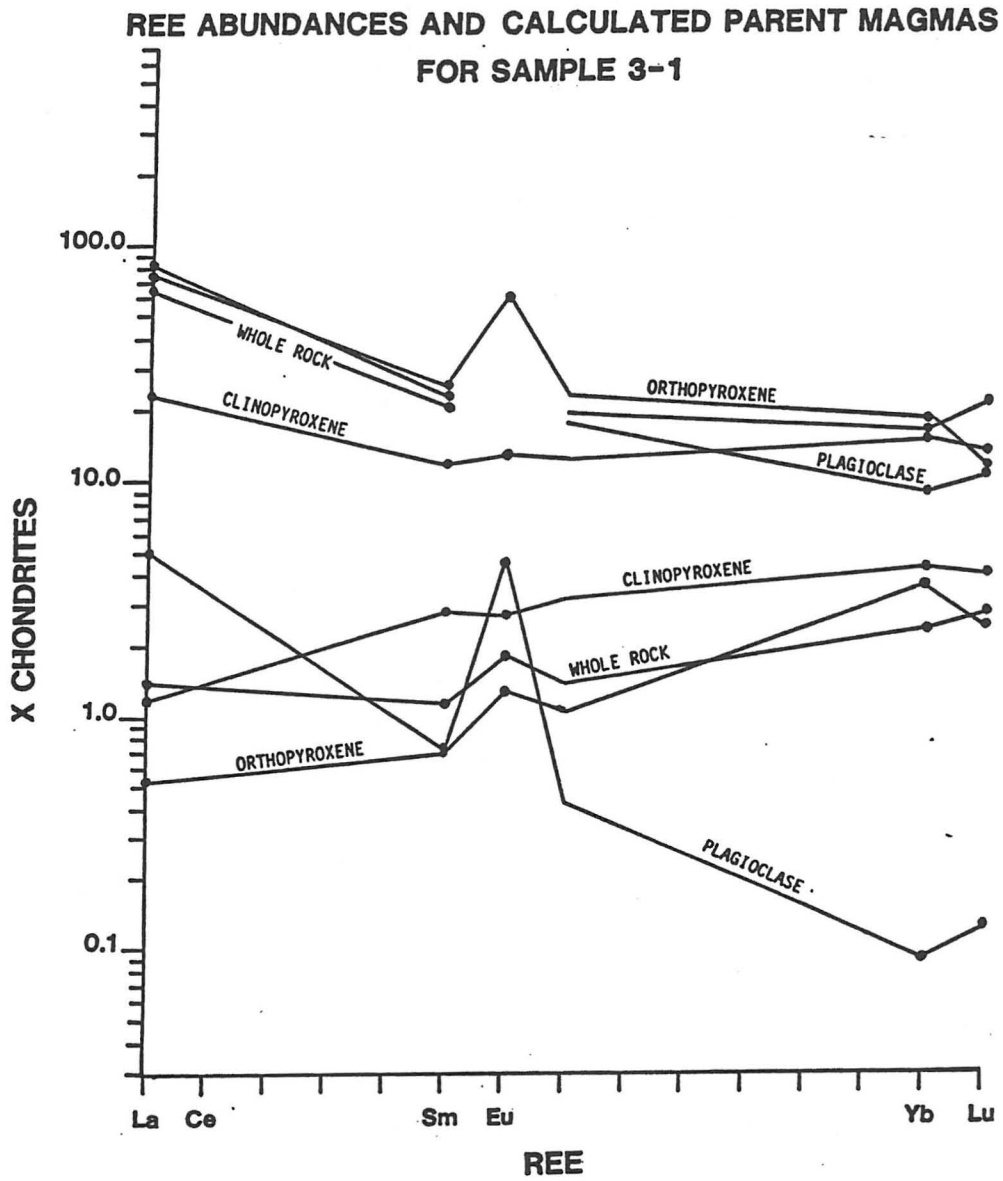

The above diagram is an example of the type of graph which results from plotting raw data (represented by the lower cluster of plotted lines) and then calculating the parental magmas based on the raw data of each phase--mineral separates and whole rock powders (upper cluster of plots). Several trends are immediately noticeable: plagioclase is depleted in heavy REE, for example. Plagioclase also shows a strong positive Europium anomaly due to the oxidation state of this element; while the other REE exist as 3+ ions, Europium can exist as a 2+ ion as well as 3+. The 2+ ion easily occupies the Ca site in the calcic plagioclase and thus produces the positive anomaly.

The upper cluster of plots are all calculations of the elemental distribution of the parent magma and theoretically should be virtually identical. Differences are probably due to the fact that there may be present some trapped magma. Other sources of error may relate to the precision of the analysis or to the distribution coefficients which may or may not suit the analysis.

CHARACTERIZATION OF PARTICLES FOUND IN HALF MILLION YEAR OLD ANTARCTIC ICE SAMPLES WITH COMPARISON TO PARTICLES COLLECTED IN THE STRATOSPHERE; S.J. Webb, Lunar and Planetary Institute, Advisor: Dr. Michael Zolensky, NASA Johnson Space Center

There is interest in refractory (high condensation temperature) interplanetary dust particles (IDP's) because these particles would be the first to condense from the early solar nebula and would yield valuable information about the conditions that existed when the solar system formed. These refractory particles should contain the minerals corundum, hibonite and perovskite (major elements : Al, Ca, Ti, Mg), as these are the first crystalline phases to occur [1]. A large variety of particles have been observed in the stratospheric dust collection and are described in the Cosmic Dust Catalogs from the Johnson Space Center [2]. Many of these particles are refractory, but have been attributed to spacecraft debris and rocket exhaust on the basis of morphology and a refractory composition. When these particles contain metastable phases, such as gamma-alumina, rather than the more stable polymorphs (corundum in this case), the particles may be definitely ascribed to spacecraft debris, since IDP's are too ancient to still contain unstable phases of this type. Also, spacecraft debris particles have not been observed to contain either hibonite or perovskite, making the identification of grains containing these minerals as IDP's very straightforward. Unfortunately, these criteria may not always be employed. Fortunately, the Antarctic ice cap contains a frozen record of atmospheric particles dating back more than one million years, and spacecraft debris particles will not be detected in ice samples that predate industrial activity.

In order to verify the extraterrestrial origin of refractory particles, samples of preindustrial ice from Antarctica have been melted and filtered to collect any particles present. There are several terrestrial sources for particles found in the ice, these include volcanic eruptions, wind-blown sand and weathering products that have settled from the atmosphere, all of which may easily be recognized from elemental and microstructural analyses. Since the ice was collected from ice fields where the ice is ablating at a fairly rapid rate (~5cm/yr) there is no danger of contamination from new ice. To ensure that the ice remained uncontaminated, the samples were collected without being touched by tools and were promptly sealed in precleaned zip-lock bags. They

were then shipped frozen and kept frozen until they were melted and filtered in a clean flow bench lab. Despite these precautions several sources of contamination exist, mainly, plastic from the bags, the containers the ice was melted in, and the plastic filter pop-tops. Aluminum foil was used to cover the melt water and is another source of contamination. Since these particles must settle through the atmosphere, atmospheric contamination is much greater than that found on particles collected in the stratosphere. There were 3 sites that the ice was collected from, the Far Western Ice Field and two distinct samples from the Allan Hills ice fields. The ice at the Far Western Ice Fields has been dated at ~100,000 years and that at the Allan Hills at ~700,000 years (Nishiizumi [3]). So far one piece of pollen has been collected which can also give dating information.

The ice was melted in clean plastic tubs on an air flow bench. The melted water was then filtered through a sequence of vertically stacked Nucleopore filters of sizes 10 and 5 microns. An attempt was made to collect smaller sized particles (1 and .4 microns) however, rapid clogging of the system made this impracticle. The filters were supported by "pop-tops" and the water drawn through them with the use of a vacume system [4]. Care was taken to keep the water from the separate sites on separate filter surfaces. When the filters became clogged they were removed and epoxied to carbon planchettes for study in the JEOL-35CF scanning electron microscope. Rapid qualitative analysies were taken to get an idea of the particles' origin. Since the majority of the particles were of volcanic (major elements Si, Al, K, Fe, Na) or of plastic (low atomic number elements only) composition and therefore of terrestrial origin, their spectrum were not saved. The search concentrated on refractory particles of possible extraterestrial origin using element maps to locate particles with concentrations of Al and Ca, two common refractory elements. Particles of appropriate composition were removed from the filters and placed on carbon grids for microstructure study in a JEOL 100C transmission electron microscope (TEM). After this study, particles of probable extraterrestrial origin will be sent out for further ion-probe studies to determine the D/H ratios and Mg-26 concentrations that will verify a cosmic origin.

To date five filters have been mapped out and partially analysed. From all of these filters particles have been found that have possible cosmic origins. These particles are currently undergoing further study in the TEM. Several particles of Ti-, Si-rich composition were found. A TEM analysis of these

showed that they were composed of rutile grains in cristobalite. It is probable, but not certain, that these particles are of volcanic origin.

The filters were kept specific to each ice collection site to see if there were any major changes in the particle types from one site to another. Therefore a qualitative temporal comparison will be performed comparing the number, type, and flux of particles between the 100,000 to 700,000 year old Antarctic ice cap and the modern stratosphere. In this way we may evaluate any possible changes in the cosmic dust type distribution through time.

REFERENCES

[1] Dodd, R.T. 1981. Meteorites: A Petrologic-Chemical Synthesis. Cambridge University Press 368pp.

[2] CDPET 1982-1985. Cosmic Dust Catalog NASA/Johnson Space Center.

[3] Nishiizumi, K. 1986. LPI Technical Report No. 86-01,71-73.

[4] Zolensky, M.E. and Mackinnon, I.D.R. , 1985, JGR,90, 5801-5808.